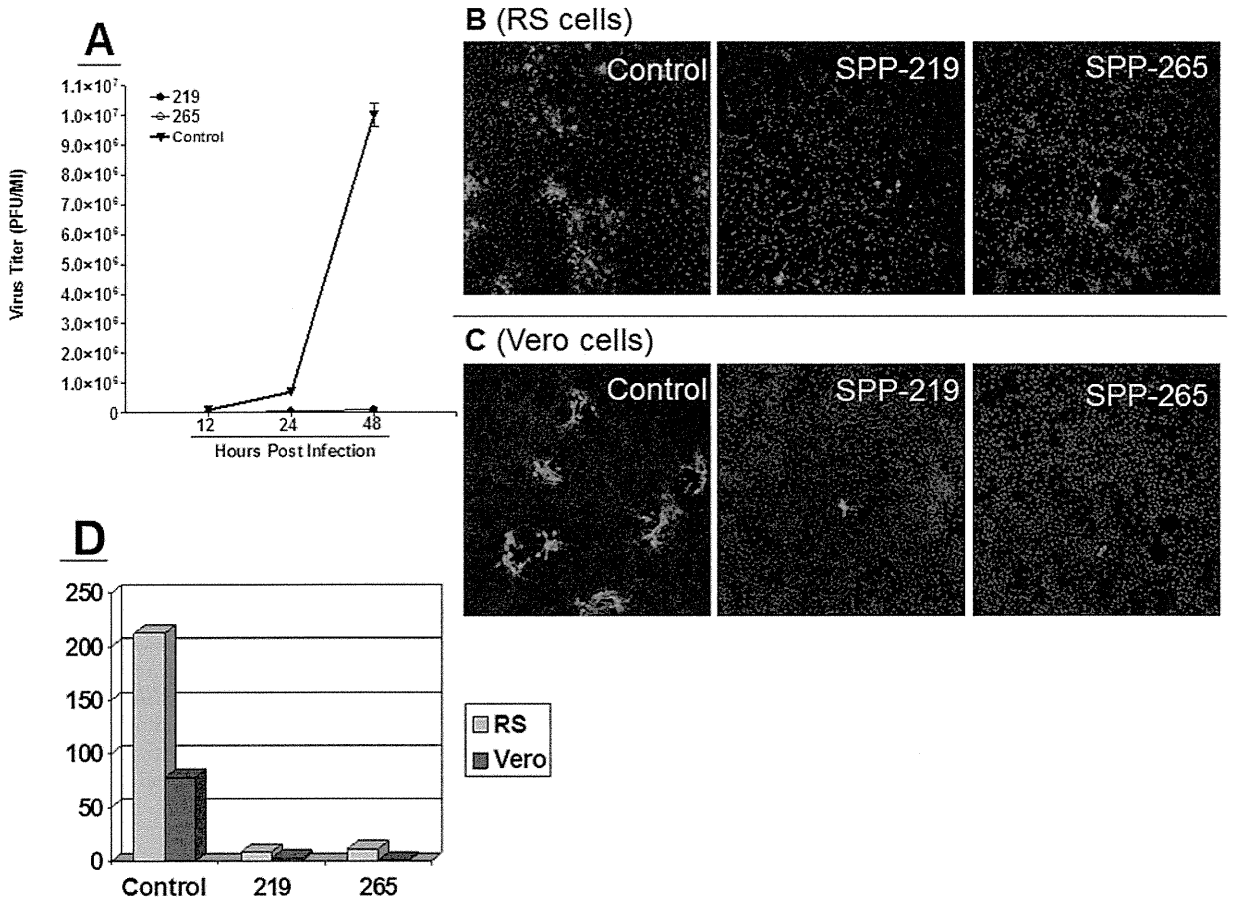

Figure 6. Blocking HSV-1 replication *in vitro* by SPP dominant negative mutants. A) Viral Titer is reduced by SPP dominant negatives. RS cells were transfected for 24 hr with either dominant negative SPP D219A, SPP 265A or wild-type SPP and infected with 0.1 PFU/cell of HSV-1 strain McKrae. Titers were measured by standard plaque assay 12, 24 and 48 hr PI. Each point represents the mean ± SEM from 3 independent experiments per time point; and B/C/D) HSV-1 protein expression is reduced by SPP knockdown. RS cells (B) and Vero cells (C) were transfected and infected as in A. At 24 hr PI, cells were stained with anti-HSV-1-gC-FITC (green) and costained with DAPI (blue). Photomicrographs are shown at 10X magnification. D) Quantification of HSV-1 positive cells from (B) and (C).
doi:10.1371/journal.pone.0085360.g006

SPP having a catalytic preference for Type II membrane proteins, SPP is able to bind to many types of preproteins, signal peptides and misfolded proteins [63]. It is in this context that SPP is associated with quality control in the ER associated degradation (ERAD) pathway [17,64]. SPP is thought to function as a membrane protease liberating burdensome protein fragments from the membrane [65,66]. The fate of these released peptides can be degradation, however their role as signaling molecules is emerging [67,68]. Under these circumstances the possibility exists that SPP also serves to liberate bioactive fragments of viral proteins including those capable of inducing gene expression. This scenario could explain the negative effects on viral gene expression we observed when SPP was reduced via shRNA.

It has also been shown that over-expression of gK in gK-transformed cells collapses the Golgi apparatus into the ER thus inhibiting virion egress, glycoprotein transport, and virus-induced cell fusion [69]. Similarly in this study we also observed physiological signs of ER stress, such as ER aggregation, in cell lines over-expressing gK. The possibility remains that the increase in glycoprotein processing within the cell during the infectious period damages the ER adding to the immunopathology caused by the virus. The implications of ER stress are well documented in human diseases such as diabetes mellitus atherosclerosis, hypoxia, neoplasia and neurodegeneration [70,71]. In addition, ER stress has been demonstrated as causative in genetic and environmental models of retinal degeneration [72]. Cells have evolved highly conserved mechanisms to deal with ER stress through the unfolded protein response (UPR) whereby functional protein processing is restored or apoptosis is induced [71,73]. In fact, HSV-1 has counter-evolved processes to sense ER stress and downregulate the UPR to maintain ER homeostasis and prevent apoptosis [74,75].

In line with the ER stress and the gK-induced collapse of the Golgi apparatus [69], we have previously shown that a recombinant HSV-1 expressing two additional copies of gK induced severe corneal scarring and dermatitis in different strains of mice [49]. Furthermore, we previously demonstrated that immunization of mice with gK, but not with any of the other known HSV-1 glycoproteins, resulted in exacerbation of CS and herpetic dermatitis following ocular HSV-1 infection [29,30]. As our results clearly demonstrate the SPP and gK can bind and colocalize with one another the possibility remains that the gK interaction with SPP may be involved in the pathology of HSV-1 induced eye disease. Consequently, this gK-SPP interaction may be considered as a specific therapeutic target for the prevention of corneal infection in patients at risk and a reduction in the severity

of the CS in patients who have established infections thereby providing an effective treatment for those suffering from the devastating effects of HSK.

Conclusion

Glycoprotein K (gK) is a hydrophobic protein and is highly conserved between HSV-1 and HSV-2. Studies using insertion/deletion mutants have shown the importance of the gK in virion morphogenesis and egress. We demonstrated previously that immunization of mice with gK, but not with any of the other HSV-1 glycoproteins, resulted in exacerbation of eye disease and herpetic dermatitis following ocular HSV-1 infection independent of mice or virus strain. We also have demonstrated that a recombinant HSV-1 expressing two extra copies of gK exacerbated eye disease in both mice and rabbit, suggesting that gK overexpression is pathogenic. In this study we have shown for the first time that: (1) HSV-1 gK binds to signal peptide peptidase (SPP); and (2) ShRNA against SPP and SPP dominant negative mutants reduced HSV-1 titers *in vitro*. Thus, blocking the interaction of gK with SPP using SPP shRNA should be considered as a potential alternative therapy in not only HSV-1, but other conditions whereby SPP processing is integral to pathogenesis.

Supporting Information

Figure S1 Results from bacerial-2-hybrid indicate SPP interacts with gK. A) BLAST results from a representative clone indicate strong consensus with all four isoforms of SPP. B) Representative sequence alignment of an isolated clone and SPP isoform 1.
(PDF)

Figure S2 c-myc-gK construct used for gK-SPP binding. The structure of the wild-type gK molecule of 338 aa is shown with an in-frame insertion of c-myc sequence on C terminus. Positions of N-glycosylation sites are indicated at AA residues 48 and 58. gK construct was inserted into the BamHI site of plasmid pcDNA3.1.
(PDF)

Figure S3 HA-SPP constructs used for gK-SPP binding and dominant negative transfection. The structure of the wt SPP molecule of 43.5 kDa is shown with an in-frame insertion of HA sequence and ER retention signal. Asp219 (D219A) and Asp265 (D265A) are SPP dominant negative mutants in which Asparagine (D) at aa positions 219 or 265 was mutated to Alanine (A) and inserted into plasmid pcDNA3.1.
(PDF)

Figure S4 SPP knockdown by shRNA construct in different cell lines. Vero, HeLa and RS cells were grown to confluency and transfected with either SPP shRNA or scramble shRNA. After 24 hr, RNA was isolated from each cell line and qRT-PCR was performed as described in Materials and Methods. SPP expression in each cell line was normalized to the scramble SPP shRNA transfected control cells. Each point represents the mean ± SEM from 3 independent experiments.
(PDF)

Figure S5 Cell vitality in presence of SPP shRNA. RS cells were transfected with SPP shRNA followed by infection with 0.1 PFU/cell of HSV-1 strain McKrae. Controls were uninfected cells and cells infected with HSV-1 without SPP shRNA. Cells were harvested 24 hr PI, stained with anti-Annexin-V antibody, and FACS analyses was performed as described in Materials and Methods. Shown is a graphical representation of the % of cells undergoing apoptosis in each group.
(PDF)

Author Contributions

Conceived and designed the experiments: HG KRM SJA. Performed the experiments: HG KRM SJA. Analyzed the data: HG SJA. Contributed reagents/materials/analysis tools: YM KM KGK. Wrote the paper: SJA HG.

References

1. Weihofen A, Binns K, Lemberg MK, Ashman K, Martoglio B (2002) Identification of signal peptide peptidase, a presenilin-type aspartic protease. Science 296: 2215–2218.
2. Lemberg MK, Martoglio B (2002) Requirements for signal peptide peptidase-catalyzed intramembrane proteolysis. Mol Cell 10: 735–744.
3. Sun H, Liu J, Ding F, Wang X, Liu M, et al. (2006) Investigation of differentially expressed proteins in rat gastrocnemius muscle during denervation-reinnervation. J Muscle Res Cell Motil 27: 241–250.
4. Bolhuis A, Matzen A, Hyyrylainen HL, Kontinen VP, Meima R, et al. (1999) Signal peptide peptidase- and ClpP-like proteins of Bacillus subtilis required for efficient translocation and processing of secretory proteins. J Biol Chem 274: 24585–24592.
5. Yan G, Zhang G, Fang X, Zhang Y, Li C, et al. (2011) Genome sequencing and comparison of two nonhuman primate animal models, the cynomolgus and Chinese rhesus macaques. Nat Biotechnol 29: 1019–1023.
6. Golde TE, Wolfe MS, Greenbaum DC (2009) Signal peptide peptidases: a family of intramembrane-cleaving proteases that cleave type 2 transmembrane proteins. Semin Cell Dev Biol 20: 225–230.
7. Urny J, Hermans-Borgmeyer I, Gercken G, Schaller HC (2003) Expression of the presenilin-like signal peptide peptidase (SPP) in mouse adult brain and during development. Gene Expr Patterns 3: 685–691.
8. Grigorenko AP, Moliaka YK, Korovaitseva GI, Rogaev EI (2002) Novel class of polytopic proteins with domains associated with putative protease activity. Biochemistry (Mosc) 67: 826–835.
9. Sato T, Nyborg AC, Iwata N, Diehl TS, Saido TC, et al. (2006) Signal peptide peptidase: biochemical properties and modulation by nonsteroidal antiinflammatory drugs. Biochemistry 45: 8649–8656.
10. Narayanan S, Sato T, Wolfe MS (2007) A C-terminal region of signal peptide peptidase defines a functional domain for intramembrane aspartic protease catalysis. J Biol Chem 282: 20172–20179.
11. Esler WP, Kimberly WT, Ostaszewski BL, Ye W, Diehl TS, et al. (2002) Activity-dependent isolation of the presenilin- gamma -secretase complex reveals nicastrin and a gamma substrate. Proc Natl Acad Sci U S A 99: 2720–2725.
12. Taniguchi Y, Kim SH, Sisodia SS (2003) Presenilin-dependent "gamma-secretase" processing of deleted in colorectal cancer (DCC). J Biol Chem 278: 30425–30428.
13. Heimann M, Roman-Sosa G, Martoglio B, Thiel HJ, Rumenapf T (2006) Core protein of pestiviruses is processed at the C terminus by signal peptide peptidase. J Virol 80: 1915–1921.
14. Li X, Chen H, Bahamontes-Rosa N, Kun JF, Traore B, et al. (2009) Plasmodium falciparum signal peptide peptidase is a promising drug target against blood stage malaria. Biochem Biophys Res Commun 380: 454–459.
15. McLauchlan J, Lemberg MK, Hope G, Martoglio B (2002) Intramembrane proteolysis promotes trafficking of hepatitis C virus core protein to lipid droplets. Embo J 21: 3980–3988.
16. Okamoto K, Moriishi K, Miyamura T, Matsuura Y (2004) Intramembrane proteolysis and endoplasmic reticulum retention of hepatitis C virus core protein. J Virol 78: 6370–6380.
17. Loureiro J, Lilley BN, Spooner E, Noriega V, Tortorella D, et al. (2006) Signal peptide peptidase is required for dislocation from the endoplasmic reticulum. Nature 441: 894–897.
18. Barron BA, Gee L, Hauck WW, Kurinij N, Dawson CR, et al. (1994) Herpetic Eye Disease Study. A controlled trial of oral acyclovir for herpes simplex stromal keratitis. Ophthalmology 101: 1871–1882.
19. Wilhelmus KR, Dawson CR, Barron BA, Bacchetti P, Gee L, et al. (1996) Risk factors for herpes simplex virus epithelial keratitis recurring during treatment of stromal keratitis or iridocyclitis. Herpetic Eye Disease Study Group. Br J Ophthalmol 80: 969–972.
20. Liesegang TJ (1999) Classification of herpes simplex virus keratitis and anterior uveitis. Cornea 18: 127–143.
21. Liesegang TJ (2001) Herpes simplex virus epidemiology and ocular importance. Cornea 20: 1–13.
22. Hill TJ (1987) Ocular pathogenicity of herpes simplex virus. Curr Eye Res 6: 1–7.
23. Dawson CR (1984) Ocular herpes simplex virus infections. Clin Dermatol 2: 56–66.

24. Dix RD (2002) Pathogenesis of herpes simplex ocular disease; Tasman W, and Jaeger, E.A., editor. Philadelphia: Lippincott, Williams and Wilkins. 1–21 p.
25. Binder PS (1984) A review of the treatment of ocular herpes simplex infections in the neonate and immunocompromised host. Cornea 3: 178–182.
26. Streilein JW, Dana MR, Ksander BR (1997) Immunity causing blindness: five different paths to herpes stromal keratitis. Immunol Today 18: 443–449.
27. Thomas J, Rouse BT (1997) Immunopathogenesis of herpetic ocular disease. Immunol Res 16: 375–386.
28. Branco BC, Gaudio PA, Margolis TP (2004) Epidemiology and molecular analysis of herpes simplex keratitis requiring primary penetrating keratoplasty. Br J Ophthalmol 88: 1285–1288.
29. Ghiasi H, Bahri S, Nesburn AB, Wechsler SL (1995) Protection against herpes simplex virus-induced eye disease after vaccination with seven individually expressed herpes simplex virus 1 glycoproteins. Invest Ophthalmol Vis Sci 36: 1352–1360.
30. Ghiasi H, Kaiwar R, Nesburn AB, Slanina S, Wechsler SL (1994) Expression of seven herpes simplex virus type 1 glycoproteins (gB, gC, gD, gE, gG, gH, and gI): comparative protection against lethal challenge in mice. J Virol 68: 2118–2126.
31. Ghiasi H, Cai S, Slanina S, Nesburn AB, Wechsler SL (1997) Nonneutralizing antibody against the glycoprotein K of herpes simplex virus type-1 exacerbates herpes simplex virus type-1-induced corneal scarring in various virus-mouse strain combinations. Invest Ophthalmol Vis Sci 38: 1213–1221.
32. Ghiasi H, Slanina S, Nesburn AB, Wechsler SL (1994) Characterization of baculovirus-expressed herpes simplex virus type 1 glycoprotein K. J Virol 68: 2347–2354.
33. McGeoch DJ, Dalrymple MA, Davison AJ, Dolan A, Frame MC, et al. (1988) The complete DNA sequence of the long unique region in the genome of herpes simplex virus type 1. J Gen Virol 69: 1531–1574.
34. Hutchinson L, Goldsmith K, Snoddy D, Ghosh H, Graham FL, et al. (1992) Identification and characterization of a novel herpes simplex virus glycoprotein, gK, involved in cell fusion. J Virol 66: 5603–5609.
35. McGeoch DJ, Cunningham C, McIntyre G, Dolan A (1991) Comparative sequence analysis of the long repeat regions and adjoining parts of the long unique regions in the genomes of herpes simplex viruses types 1 and 2. J Gen Virol 72: 3057–3075.
36. Dolan A, Jamieson FE, Cunningham C, Barnett BC, McGeoch DJ (1998) The genome sequence of herpes simplex virus type 2. J Virol 72: 2010–2021.
37. St Leger AJ, Peters B, Sidney J, Sette A, Hendricks RL (2011) Defining the herpes simplex virus-specific CD8+ T cell repertoire in C57BL/6 mice. J Immunol 186: 3927–3933.
38. Jing L, Haas J, Chong TM, Bruckner JJ, Dann GC, et al. (2012) Cross-presentation and genome-wide screening reveal candidate T cells antigens for a herpes simplex virus type 1 vaccine. J Clin Invest 122: 654–673.
39. David AT, Baghian A, Foster TP, Chouljenko VN, Kousoulas KG (2008) The herpes simplex virus type 1 (HSV-1) glycoprotein K(gK) is essential for viral corneal spread and neuroinvasiveness. Curr Eye Res 33: 455–467.
40. Debroy C, Pederson N, Person S (1985) Nucleotide sequence of a herpes simplex virus type 1 gene that causes cell fusion. Virology 145: 36–48.
41. Bond VC, Person S (1984) Fine structure physical map locations of alterations that affect cell fusion in herpes simplex virus type 1. Virology 132: 368–376.
42. Little SP, Schaffer PA (1981) Expression of the syncytial (syn) phenotype in HSV-1, strain KOS: genetic and phenotypic studies of mutants in two syn loci. Virology 112: 686–702.
43. Pogue-Geile KL, Spear PG (1987) The single base pair substitution responsible for the Syn phenotype of herpes simplex virus type 1, strain MP. Virology 157: 67–74.
44. Foster TP, Kousoulas KG (1999) Genetic analysis of the role of herpes simplex virus type 1 glycoprotein K in infectious virus production and egress. J Virol 73: 8457–8468.
45. Hutchinson L, Johnson DC (1995) Herpes simplex virus glycoprotein K promotes egress of virus particles. J Virol 69: 5401–5413.
46. Hutchinson L, Roop-Beauchamp C, Johnson DC (1995) Herpes simplex virus glycoprotein K is known to influence fusion of infected cells, yet is not on the cell surface. J Virol 69: 4556–4563.
47. Jayachandra S, Baghian A, Kousoulas KG (1997) Herpes simplex virus type 1 glycoprotein K is not essential for infectious virus production in actively replicating cells but is required for efficient envelopment and translocation of infectious virions from the cytoplasm to the extracellular space. J Virol 71: 5012–5024.
48. Melancon JM, Luna RE, Foster TP, Kousoulas KG (2005) Herpes simplex virus type 1 gK is required for gB-mediated virus-induced cell fusion, while neither gB and gK nor gB and UL20p function redundantly in virion de-envelopment. J Virol 79: 299–313.
49. Mott KR, Perng GC, Osorio Y, Kousoulas KG, Ghiasi H (2007) A Recombinant Herpes Simplex Virus Type 1 Expressing Two Additional Copies of gK Is More Pathogenic than Wild-Type Virus in Two Different Strains of Mice. J Virol 81: 12962–12972.
50. Mott KR, Osorio Y, Maguen E, Nesburn AB, Wittek AE, et al. (2007) Role of anti-glycoproteins D (anti-gD) and K (anti-gK) IgGs in pathology of herpes stromal keratitis in humans. Invest Ophthalmol Vis Sci 48: 2185–2193.
51. Perng GC, Dunkel EC, Geary PA, Slanina SM, Ghiasi H, et al. (1994) The latency-associated transcript gene of herpes simplex virus type 1 (HSV-1) is required for efficient in vivo spontaneous reactivation of HSV-1 from latency. J Virol 68: 8045–8055.
52. Foster TP, Alvarez X, Kousoulas KG (2003) Plasma membrane topology of syncytial domains of herpes simplex virus type 1 glycoprotein K (gK): the UL20 protein enables cell surface localization of gK but not gK-mediated cell-to-cell fusion. J Virol 77: 499–510.
53. Altschul SF, Gish W, Miller W, Myers EW, Lipman DJ (1990) Basic local alignment search tool. J Mol Biol 215: 403–410.
54. Allen SJ, Hamrah P, Gate DM, Mott KR, Mantopoulos D, et al. (2011) The role of LAT in increased CD8+ T cell exhaustion in trigeminal ganglia of mice latently infected with herpes simplex virus type 1. J Virol 85: 4184–4197.
55. Randall G, Panis M, Cooper JD, Tellinghuisen TL, Sukhodolets KE, et al. (2007) Cellular cofactors affecting hepatitis C virus infection and replication. Proc Natl Acad Sci U S A 104: 12884–12889.
56. Okamoto K, Mori Y, Komoda Y, Okamoto T, Okochi M, et al. (2008) Intramembrane processing by signal peptide peptidase regulates the membrane localization of hepatitis C virus core protein and viral propagation. J Virol 82: 8349–8361.
57. Chouljenko VN, Iyer AV, Chowdhury S, Kim J, Kousoulas KG (2010) The herpes simplex virus type 1 UL20 protein and the amino terminus of glycoprotein K (gK) physically interact with gB. J Virol 84: 8596–8606.
58. Foster TP, Chouljenko VN, Kousoulas KG (2008) Functional and physical interactions of the herpes simplex virus type 1 UL20 membrane protein with glycoprotein K. J Virol 82: 6310–6323.
59. Mo C, Holland TC (1997) Determination of the transmembrane topology of herpes simplex virus type 1 glycoprotein K. J Biol Chem 272: 33305–33311.
60. Ramaswamy R, Holland TC (1992) In vitro characterization of the HSV-1 UL53 gene product. Virology 186: 579–587.
61. Beel AJ, Sanders CR (2008) Substrate specificity of gamma-secretase and other intramembrane proteases. Cell Mol Life Sci 65: 1311–1334.
62. Jambunathan N, Chowdhury S, Subramanian R, Chouljenko VN, Walker JD, et al. (2011) Site-specific proteolytic cleavage of the amino terminus of herpes simplex virus glycoprotein K on virion particles inhibits virus entry. J Virol 85: 12910–12918.
63. Schrul B, Kapp K, Sinning I, Dobberstein B (2010) Signal peptide peptidase (SPP) assembles with substrates and misfolded membrane proteins into distinct oligomeric complexes. Biochem J 427: 523–534.
64. Crawshaw SG, Martoglio B, Meacock SL, High S (2004) A misassembled transmembrane domain of a polytopic protein associates with signal peptide peptidase. Biochem J 384: 9–17.
65. Schenk D (2000) Alzheimer's disease. A partner for presenilin. Nature 407: 34–35.
66. Kopan R, Ilagan MX (2004) Gamma-secretase: proteasome of the membrane? Nat Rev Mol Cell Biol 5: 499–504.
67. Weihofen A, Martoglio B (2003) Intramembrane-cleaving proteases: controlled liberation of proteins and bioactive peptides. Trends Cell Biol 13: 71–78.
68. Martoglio B, Dobberstein B (1998) Signal sequences: more than just greasy peptides. Trends Cell Biol 8: 410–415.
69. Foster TP, Rybachuk GV, Alvarez X, Borkhsenious O, Kousoulas KG (2003) Overexpression of gK in gK-transformed cells collapses the Golgi apparatus into the endoplasmic reticulum inhibiting virion egress, glycoprotein transport, and virus-induced cell fusion. Virology 317: 237–252.
70. Marciniak SJ, Ron D (2006) Endoplasmic reticulum stress signaling in disease. Physiol Rev 86: 1133–1149.
71. Xu C, Bailly-Maitre B, Reed JC (2005) Endoplasmic reticulum stress: cell life and death decisions. J Clin Invest 115: 2656–2664.
72. Kroeger H, Messah C, Ahern K, Gee J, Joseph V, et al. (2012) Induction of Endoplasmic Reticulum Stress Genes, BiP and Chop, in Genetic and Environmental Models of Retinal Degeneration. Invest Ophthalmol Vis Sci 53: 7590–7599.
73. Wu J, Kaufman RJ (2006) From acute ER stress to physiological roles of the Unfolded Protein Response. Cell Death Differ 13: 374–384.
74. Burnett HF, Audas TE, Liang G, Lu RR (2012) Herpes simplex virus-1 disarms the unfolded protein response in the early stages of infection. Cell Stress Chaperones 17: 473–483.
75. Mulvey M, Arias C, Mohr I (2007) Maintenance of endoplasmic reticulum (ER) homeostasis in herpes simplex virus type 1-infected cells through the association of a viral glycoprotein with PERK, a cellular ER stress sensor. J Virol 81: 3377–3390.

SCIENTIFIC REPORTS

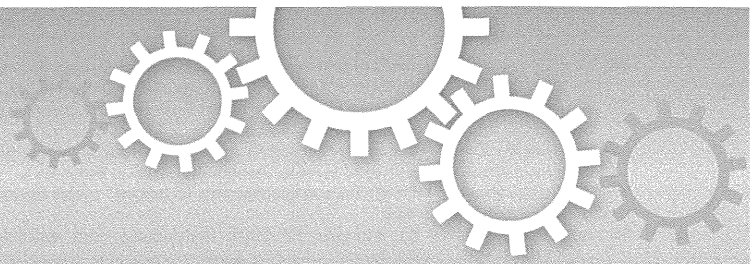

OPEN

SUBJECT AREAS:
HIGH-THROUGHPUT SCREENING
ASSAY SYSTEMS
SINGLE-CELL IMAGING
LAB-ON-A-CHIP

Received
20 September 2013

Accepted
10 February 2014

Published
28 February 2014

Correspondence and requests for materials should be addressed to N.Y. (n-yosi44@agr.nagoya-u.ac.jp) or S.K. (skuroda@agr.nagoya-u.ac.jp)

High-throughput *de novo* screening of receptor agonists with an automated single-cell analysis and isolation system

Nobuo Yoshimoto[1], Kenji Tatematsu[2], Masumi Iijima[1], Tomoaki Niimi[1], Andrés D. Maturana[1], Ikuo Fujii[3], Akihiko Kondo[4], Katsuyuki Tanizawa[2] & Shun'ichi Kuroda[1]

[1]Graduate School of Bioagricultural Sciences, Nagoya University, Furo-cho, Chikusa-ku, Nagoya, Aichi 464-8601, Japan, [2]The Institute of Scientific and Industrial Research, Osaka University, Mihogaoka, Ibaraki, Osaka 567-0047, Japan, [3]Graduate School of Science, Osaka Prefecture University, Gakuen-cho, Naka-ku, Sakai, Osaka 599-8570, Japan, [4]Graduate School of Engineering, Kobe University, Rokkodai-cho, Nada-ku, Kobe, Hyogo 657-8501, Japan.

Reconstitution of signaling pathways involving single mammalian transmembrane receptors has not been accomplished in yeast cells. In this study, intact EGF receptor (EGFR) and a cell wall-anchored form of EGF were co-expressed on the yeast cell surface, which led to autophosphorylation of the EGFR in an EGF-dependent autocrine manner. After changing from EGF to a conformationally constrained peptide library, cells were fluorescently labeled with an anti-phospho-EGFR antibody. Each cell was subjected to an automated single-cell analysis and isolation system that analyzed the fluorescent intensity of each cell and automatically retrieved each cell with the highest fluorescence. In ~3.2×10^6 peptide library, we isolated six novel peptides with agonistic activity of the EGFR in human squamous carcinoma A431 cells. The combination of yeast cells expressing mammalian receptors, a cell wall-anchored peptide library, and an automated single-cell analysis and isolation system might facilitate a rational approach for *de novo* drug screening.

Sensing of extracellular ligands (*e.g.*, hormones, cytokines and growth factors) *via* receptors on the cell surface modulates intracellular signaling molecules and subsequently regulates gene expression. Analysis of receptor-mediated signal transduction allows delineation of signaling pathways involved in the onset of various diseases. Thus, it is important to find or design drugs with agonistic or antagonistic activity for target receptors.

To date, seven transmembrane G-protein-coupled receptors (GPCRs) have been recognized as potential target molecules for drug discovery (*e.g.*, propranolol as an antagonist of β-adrenergic receptors, phenylephrine as an agonist of α1-adrenergic receptor)[1,2]. Single transmembrane receptor tyrosine kinases (RTKs) are also potential therapeutic targets. After conventional screening for drugs that bind to RTKs on mammalian cells, molecular target drugs have been developed to modulate these receptors, particularly for the purpose of treating cancers (*e.g.*, gefitinib as an antagonist of the epidermal growth factor receptor (EGFR)[3], trastuzumab as an antagonist of HER2 (a member of EGFR family)[4]). For drug discovery, it is indispensable to prepare a tremendous number of chemical compounds ($10^4 \sim 10^5$ species) to identify lead compounds that target receptors. Because the initial screening is usually undertaken by *in vitro* administration of each chemical compound to mammalian cells (*e.g.*, Chinese hamster ovary cells over-expressing target receptors), it is laborious to evaluate compounds using a large number of cell cultures. Furthermore, endogenous regulation mechanisms of target receptors, such as redundancy, crosstalk and feedback[5–7], may affect quantitative measurement of second messenger levels[8–10]. These situations led us to develop a new high-throughput screening system of drugs for target receptors without any interference from endogenous regulation mechanisms.

Because *Saccharomyces cerevisiae* expresses two endogenous GPCRs, STE2 and STE3[11], various mammalian GPCRs have been successfully expressed in *S. cerevisiae* (*e.g.*, adrenergic, chemoattractant C5a, serotonin and somatostatin receptors)[12]. Some mammalian GPCRs activate the yeast pheromone-sensing pathway in a dose-dependent manner of each ligand[13,14], suggesting that yeast is suitable for quantitative analyses of mammalian GPCRs and their ligands. For example, Klein *et al.*[15] succeeded in *de novo* screening of agonists for the human formyl peptide receptor like-1 receptor (FPRL-1R) using yeast cells co-expressing FPRL-1R and a random peptide library. Yeast cells are also considered as suitable host cells for screening agonists and antagonists of RTKs,

because there is no tyrosine kinase activity in yeast cells[16]. When a constitutively active EGFR is expressed on the yeast cell surface, the EGFR autophosphorylates and recruits Grb2 and Sos near the yeast plasma membrane, followed by activation of the Ras signaling pathway[17]. However, EGF-dependent activation of the EGFR (*i.e.*, autophosphorylation) has not been detected in yeast cells, probably because the yeast cell wall prevents EGF from accessing the ligand-binding domain of the EGFR.

Here, we report that a cell wall-anchored form of EGF can access the EGFR expressed on the yeast cell surface, and EGF activates the EGFR in an autocrine manner. Furthermore, a cell wall-anchored form of a conformationally constrained peptide library[18], instead of EGF, allowed us to develop a *de novo* high-throughput screening system of agonists for the EGFR. In this system, yeast cells were stained by indirect immunofluorescence with an anti-phospho-EGFR antibody, and then analyzed with an automated single-cell analysis and isolation system[19]. Finally, in the $\sim 3.2 \times 10^6$ peptide library, we have identified six novel peptides that show agonistic activity of the EGFR in mammalian cells for a short period.

Results

EGF-dependent autophosphorylation of the EGFR in yeast cells. Because the yeast cell wall prevents extracellular macromolecules from accessing the plasma membrane[13,14,17], both EGF and the EGFR were concurrently displayed on the yeast cell surface to increase the local concentration of EGF for reconstitution of the EGF signaling pathway in yeast cells (Figure 1a). An N-terminal HA-epitope-tagged human EGF was expressed in the periplasm with the assistance of MFα1-prepro peptide[20] and FLO42 (cell wall-anchoring domain of FLO1[21]) (Figure 1b, top). A C-terminal V5-epitope-tagged human EGFR was expressed as a membrane-anchored form with the assistance of SUC2-signal peptide[22] (Figure 1b, bottom). Western blot analysis showed that HA-EGF-FLO42 and EGFR-V5 were localized in cell wall and cytosolic fractions, respectively (Figure 1c). Because the calculated molecular weight of mature HA-EGF-FLO42 was 11,783, the faint 12 kDa band and broad >20 kDa bands (left panel) were considered as non-glycosylated and glycosylated forms of HA-EGF-FLO42, respectively. In addition, the calculated molecular weight of mature EGFR-V5 was 133,901, and the broad 130 and 160 kDa bands (right panel) might have corresponded to non-glycosylated and glycosylated forms of EGFR-V5, respectively. The size of the latter band corresponded well with that of the EGFR expressed in mammalian cells. Indirect immunofluorescence analyses using confocal laser scanning microscopy (LSM) indicated that HA-EGF-FLO42 was successfully localized on the yeast cell surface (Figure 1d). After treatment with zymolyase, spheroplasts were also subjected to indirect immunofluorescence analyses that indicated that EGFR-V5 resided mainly in the yeast plasma membrane and partly in the cytoplasm (Figure 1e).

Localization of HA-EGF-FLO42 and EGFR-V5 on the yeast cell surface (*see* Figure 1d and e) suggested that the EGFR was autophosphorylated by adjacent EGF in an autocrine manner. After incubation in HEPES buffer (pH 7.0) for 1 h to facilitate an efficient interaction between the EGFR and EGF, the fractions of cytoplasm and cell wall of yeast cells were prepared, and then analyzed with anti-EGFR phosphotyrosine (pY) antibodies against pY-1068, pY-1148 and pY-1173 (Figure 2a). EGFR expressed in yeast cells was found to be phosphorylated by the co-expression of HA-EGF-FLO42 (lane 3), which was reduced by the treatment with tyrphostin AG1478[23], a specific inhibitor for EGFR autophosphorylation (lane 4). Next, yeast cells were treated with zymolyase, and spheroplasts were probed with the anti-EGFR pY antibodies. Fluorescence derived from each phosphotyrosine was observed in cell peripheries (Figure 2c–e, left panels). Flow cytometric analyses confirmed that spheroplasts harboring phosphorylated EGFRs were substantially increased in an EGF-dependent manner (Figure 2c–e, right panels), whereas cell surface display of human interleukin-5 (HA-IL5-FLO42) (Figure 2b), a non EGFR-related protein, could not induce the phosphorylation of EGFR. Since anti-EGFR pY-1173 antibody showed good signal to noise ratio in western blot and flow cytometric analyses, we selected the antibody for further analyses. Taken together, cell surface engineering facilitated, for the first time, detection of EGF-dependent autophosphorylation of the EGFR in yeast cells, which allowed us to develop a new system to analyze ligand interactions with various receptors including RTKs and GPCRs without any interference from other mammalian proteins.

EGF-dependent homo-oligomerization of the EGFR in the yeast plasma membrane. As observed in mammalian cells[24], autophosphorylation of the EGFR upon EGF-binding suggested homo-oligomer formation of EGFRs in the yeast plasma membrane. A split-ubiquitin (ub) membrane two-hybrid assay[25] was carried out with the *S. cerevisiae* NMY51 strain harboring *Lacz* and *HIS3* reporter genes under the control of the LexA-driven promoter using bait EGFR fused with the C-terminal half of ub (Cub) and a LexA-VP16 hybrid transcription factor (DNA-binding domain of LexA and transactivating domain of herpes simplex virus VP16) (EGFR-Cub-LexA-VP16), and prey EGFR fused with the N-terminal half of ub (Nub) (EGFR-Nub) (Supplementary Figure S1a). When ub was reconstituted upon oligomerization of the EGFR, the linkage between Cub and LexA was digested by endogenous ub C-terminal hydrolase, followed by release of LexA-VP16. By co-expression with HA-EGF-FLO42, yeast cells could grow on His-depleted plates and turn blue on X-gal-containing plates (Supplementary Figure S1b). These results indicated that EGF displayed on the yeast cell surface remarkably induced homo-oligomerization of EGFRs in the yeast plasma membrane.

Functional interaction of the EGFR with Grb2 and Shc1. By expressing constitutively active EGFR in yeast cells, autophosphorylated EGFRs recruited exogenous Grb2, Shc1 and Sos to the plasma membrane, followed by activation of the yeast RAS signaling pathway[17]. Therefore, we introduced HA-EGF-FLO42 and EGFR-V5 into a temperature-sensitive mutant of the *S. cerevisiae* cdc25h strain[26] co-expressing the Sos-fused form of Grb2 or Shc1 (Supplementary Figure S2a). The cdc25h strain harbors temperature-sensitive CDC25 ($CDC25^{ts}$) that functions as a GDP-GTP exchanging factor for RAS1 and RAS2, and induces growth inhibition at 37°C. When the EGFR was activated by EGF, yeast cells survived even at 37°C due to complementation of the function of $CDC25^{ts}$ by Grb2-Sos or Shc1-Sos (Supplementary Figure S2b). In control yeast cells expressing FLO42 instead of HA-EGF-FLO42, almost no cells could grow at 37°C. These results indicated that the yeast RAS signaling pathway was effectively activated by EGF-dependent EGFR autophosphorylation.

High-throughput *de novo* screening of EGFR agonists by an automated single-cell analysis and isolation system. Recently, we have developed an automated single-cell analysis and isolation system that isolates single cells of interest from arrays containing large number of cells[19]. Based on the functional interaction between EGF and the EGFR on the yeast cell surface, a conformationally constrained peptide library, instead of HA-EGF-FLO42, was introduced into yeast cells for *de novo* screening of EGFR agonists. The peptide library consisted of MFα1-prepro peptide, helix-loop-helix (HLH), FLAG-epitope tag and FLO42 from the N- to C-terminals (Figure 3a). The HLH moiety was composed of two helixes split by a hepta-glycine (G_7)-loop, in which the C-terminal helix contained randomized sequences of five amino acids (approximately 3.2×10^6 variations) on its solvent-accessible surface[17]. Cells containing the peptide library were subjected to indirect immunofluorescence analysis with an anti-FLAG antibody

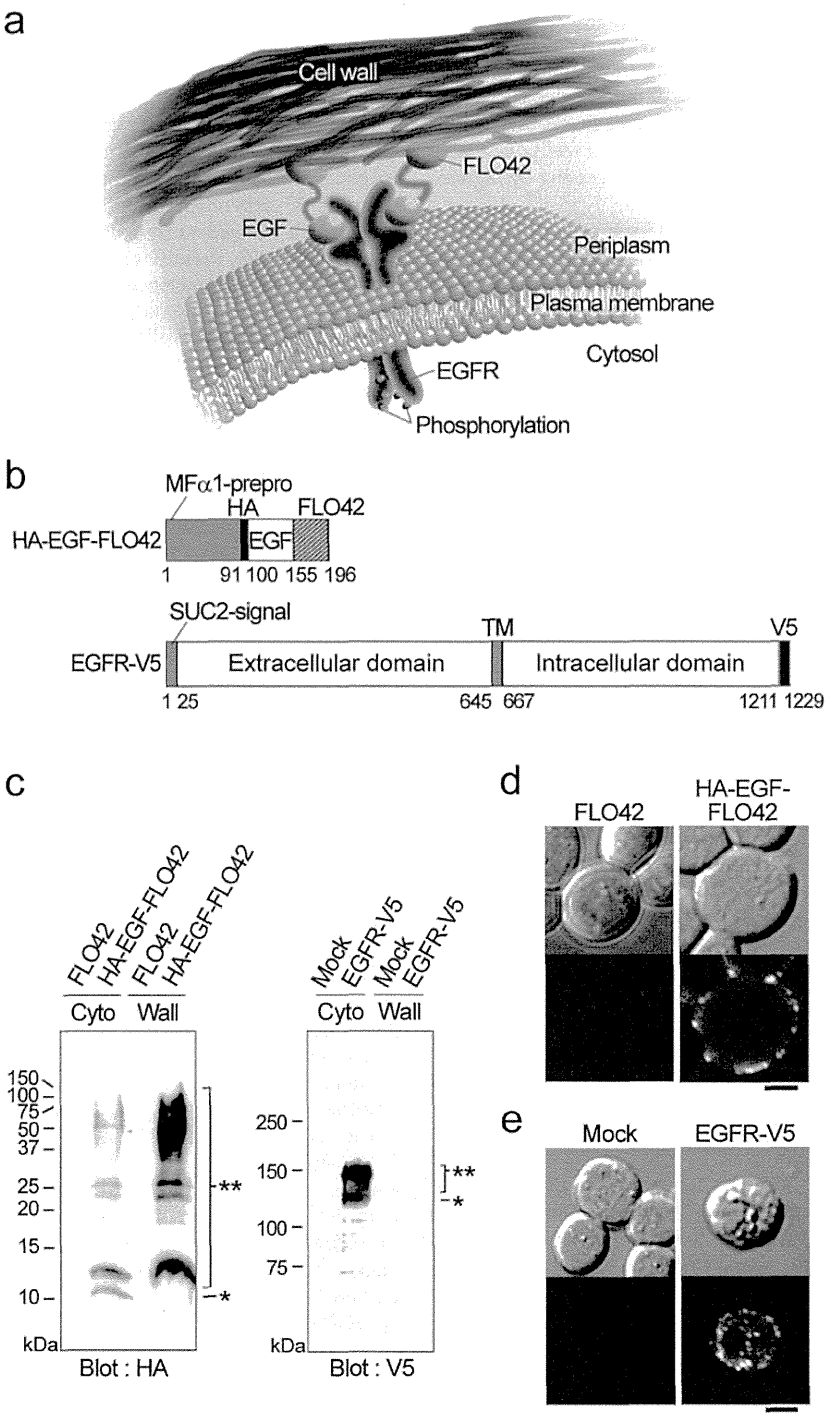

Figure 1 | Expression and subcellular localization of the EGF-FLO42 and EGFR in yeast cells. (a) Schematic drawing of the EGFR and FLO42-fused EGF in the periplasm of yeast cells. Upon binding EGF, the EGFR autophosphorylates. (b) A cell wall-anchored form of HA-tagged EGF (HA-EGF-FLO42) was expressed with the assistance of MFα1-prepro peptide. V5-tagged human EGFR (EGFR-V5) was expressed with the assistance of SUC2-signal peptide. *TM*, transmembrane domain. Numbers indicate amino acid residues at the borders of each domain. (c) Co-expression of HA-EGF-FLO42 and EGFR-V5 in yeast cells. Cytoplasmic (*Cyto*) and cell-wall (*Wall*) fractions were analyzed by western blotting using anti-HA (*HA*) and anti-V5 (*V5*) antibodies. Single and double asterisks indicate non-glycosylated and glycosylated forms, respectively. (d) Subcellular localization of HA-EGF-FLO42 in yeast cells. Intact cells were stained with anti-HA antibody. *Bars* = 2 μm. (e) Subcellular localization of EGFR-V5 in yeast cells. Spheroplasts were stained with anti-V5 antibody. *Bars* = 2 μm.

and then observed by confocal LSM. Fluorescence was observed around the periphery of yeast cells (Figure 3b), similar to HA-EGF-FLO42 (*see* Figure 1d), indicating that the peptide library was efficiently displayed on the yeast cell surface. Meanwhile, based on the flow cytometric analyses, about 100% of yeast cells expressed both HLH-FLAG-FLO42 library and EGFR-V5 concurrently, suggesting that randomized HLH peptide library could be screened thoroughly in yeast cell expressing EGFR-V5.

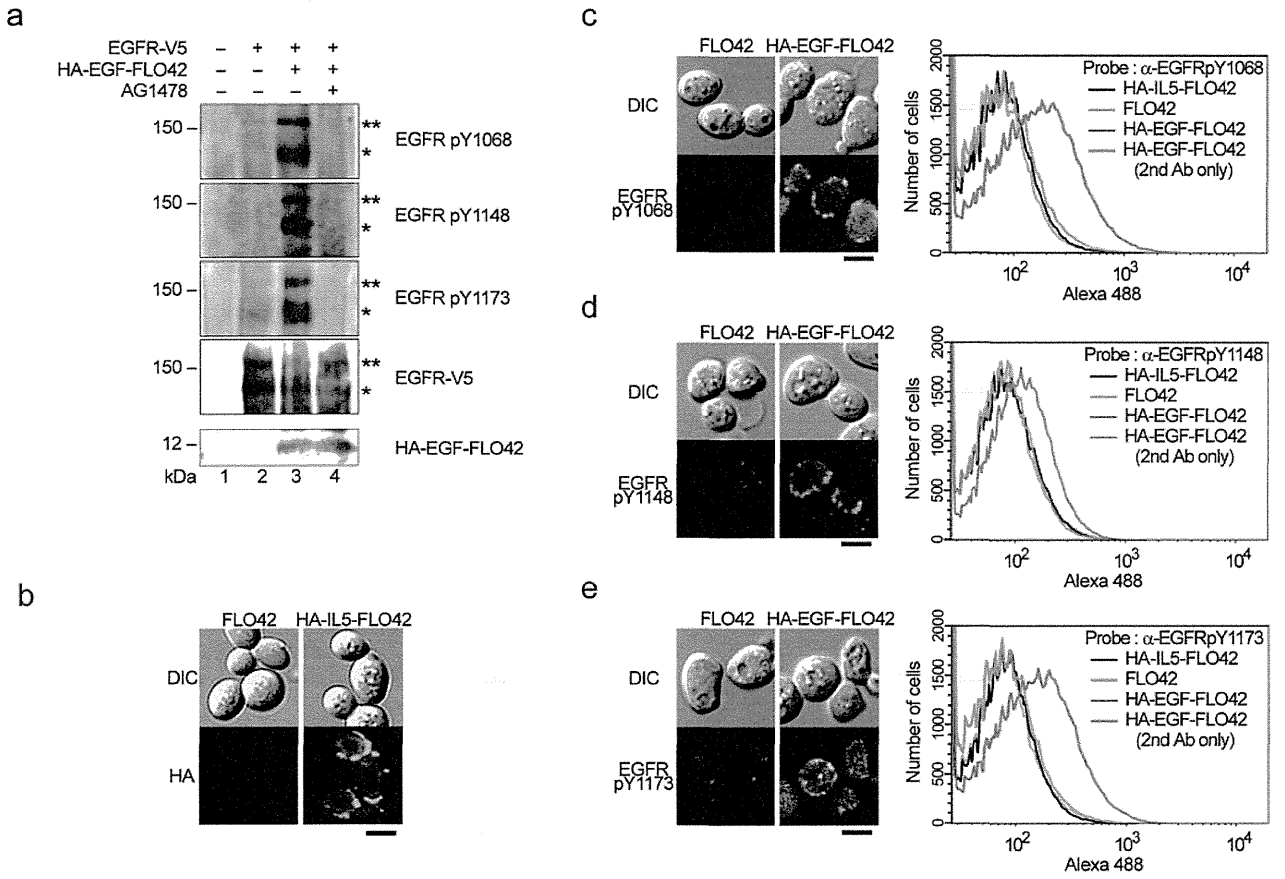

Figure 2 | Autophosphorylation of EGFR-V5 induced by HA-EGF-FLO42 in yeast cells. (a) EGF-dependent autophosphorylation of EGFR. Yeast cells co-expressing HA-EGF-FLO42 and EGFR-V5 were lysed and separated to cytoplasmic and cell wall fractions. Cytoplasmic fraction was subjected to western blot analysis using anti-V5 and anti-EGFR antibodies against phosphotyrosine-1068 (pY-1068), pY-1148 and pY-1173. Expression of HA-EGF-FLO42 in cell wall fraction was confirmed by using anti-HA antibody. Numbers shown at the bottom indicate lane number. Single and double asterisks indicate non-glycosylated and glycosylated forms, respectively. (b) Subcellular localization of HA-IL5-FLO42 in yeast cells. Intact cells were stained with anti-HA antibody. *Bar* = 2 μm. (c–e) Autophosphorylation of EGFR-V5 induced by HA-EGF-FLO42 in yeast cells. Spheroplasts were stained with a specific antibody against pY-1068 (c), pY-1148 (d) and pY-1173 (e) in the EGFR, and then subjected to microscopic and flow cytometric analyses. HA-IL5-FLO42 was used as control of non-specific ligand for EGFR. *Bars* = 2 μm.

Yeast cells co-expressing the peptide library and EGFR were cultured for 16 h, incubated in HEPES buffer (pH 7.0) for 1 h, fixed with 4% PFA, treated with zymolyase, stained by indirect immunofluorescence with an anti-EGFR pY-1173 antibody, and then placed into microchambers (a polystyrene slide containing 2.5×10^5 of 10-μm wells) by gentle centrifugation. About 80 ~ 90% of wells contained one to two spheroplasts. The fluorescent intensity and position of each spheroplast were analyzed by the automated single-cell analysis and isolation system (Figure 3c). After identifying positive spheroplasts with high fluorescent intensities, they were automatically retrieved with a glass capillary and individually transferred into the wells of a 96-well PCR plate. Finally, from approximately 5×10^6 spheroplasts (3.2×10^6 independent clones), 83 positive spheroplasts were isolated and their fluorescent intensity was already sorted in descending order.

Evaluation of EGFR agonist candidates in A431 cells. Using single cell-based PCR, 65 DNA fragments encoding the HLH moiety were successfully amplified from 83 positive spheroplasts (Figure 4a). Among 13 clones with high fluorescent intensities, DNA sequencing revealed that four (clones 2, 6, 9 and 10) and three clones (clones 8, 11 and 12) encoded identical amino acid sequences, respectively (Supplementary Tables S1 and S2). Eight clones encoding distinct amino acid sequences were expressed as an N-terminal thioredoxin-fused C-terminal hexahistidine-tagged form in *Escherichia coli* BL21 (DE3) (Figure 4b), and fused proteins were purified with a cobalt-chelating column (Figure 4c). These proteins were added to the culture medium of human adenosquamous carcinoma A431 cells that overexpress the EGFR. Western blot analysis using an anti-EGFR antibody against pY-1173 demonstrated that six proteins (derived from clones 2, 3, 5, 7, 8 and 13) possessed an agonistic activity for the EGFR in mammalian cells (Figure 5a), which was estimated less than 0.1% of EGF (working concentration, 1.5 nM for EGF versus 2.0 μM for peptides) (Figure 5b). However, the agonistic activity of each peptide was completely inhibited by the treatment with tyrphostin AG1478, corroborating that each peptide functions as an EGFR agonist.

Discussion

Here, we demonstrated that the EGFR expressed in the yeast plasma membrane could form homo-oligomers upon stimulation with cell wall-anchored EGF, followed by its autophosphorylation and activation of the yeast RAS signaling pathway. This is the first report of yeast cells that can reconstitute a mammalian growth-signaling pathway mediated by the EGF-EGFR-Grb2/Shc1-Sos-Ras complex. By replacing EGF with a random peptide library, we achieved high-throughput screening of EGFR agonists using an automated

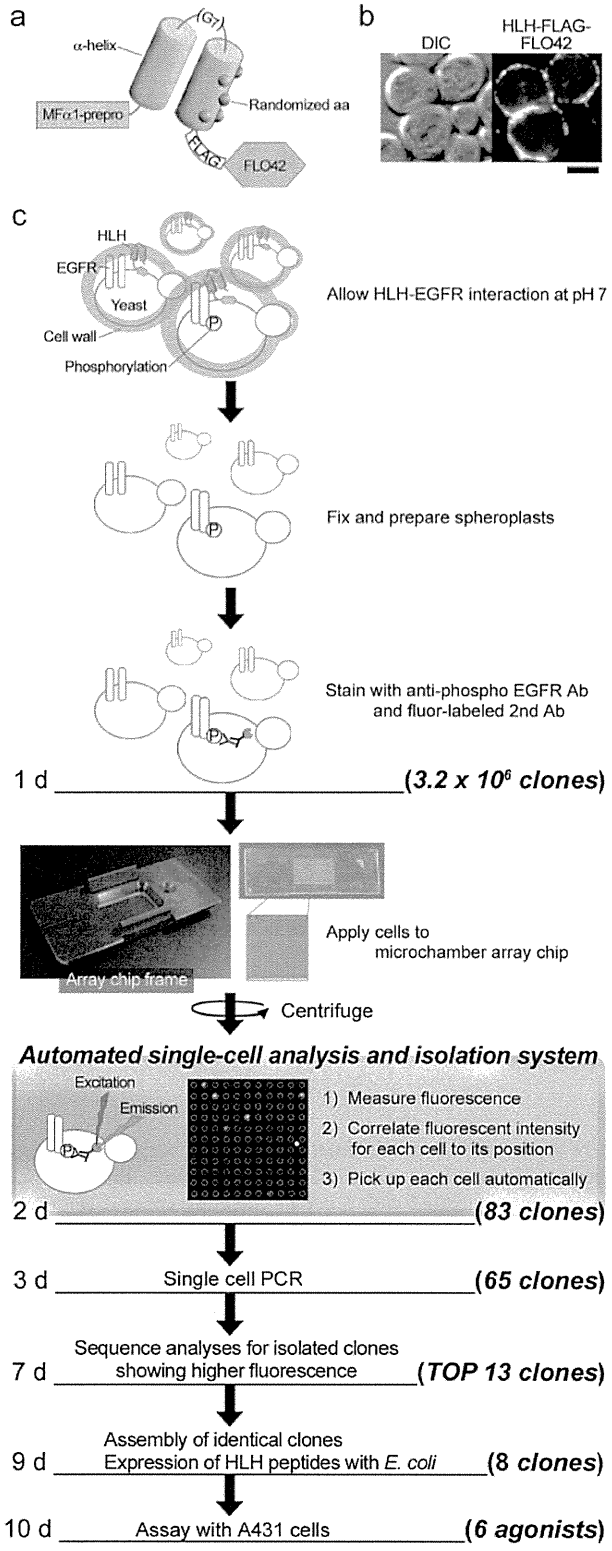

Figure 3 | High-throughput *de novo* screening of EGFR agonists. (a) A cell wall-anchored form of FLAG-tagged HLH (HLH-FLAG-FLO42) was expressed with the assistance of MFα1-prepro peptide. The HLH consisted of two α-helixes (blue cylinders) linked with a hepta-glycine (G_7) loop, in which the second α-helix contained randomized sequences of five amino acids (red dots) on its solvent-accessible surface. (b) Subcellular localization of HLH-FLAG-FLO42 in yeast cells. Intact cells were stained with an anti-FLAG antibody. *Bar* = 2.5 μm. (c) Flowchart of EGFR agonist screening. Approximately 3.2×10^6 cells co-expressing HLH-FLAG-FLO42 (*HLH*) and EGFR-V5 (*EGFR*) were incubated at pH 7 for 1 h, fixed with paraformaldehyde and then treated with zymolyase, followed by incubation with an anti-phospho EGFR antibody. Approximately 2.5×10^5 cells were individually placed into the microchambers of cell array chip by brief centrifugation. The chip was scanned with a CCD camera under UV light by an automated single-cell analysis and isolation system. In the microchamber array chip, positive and negative cells were indicated by red and green circles, respectively. Positive cells were automatically retrieved with a glass capillary equipped on the micromanipulator. Using 20 chips, 83 positive cells were obtained, and 65 DNA fragments were amplified by single cell-based PCR. Amino acid sequences were deduced from 13 fragments derived from cells with high fluorescence and then aligned. Finally, eight independent EGFR agonist candidates were obtained, synthesized in *E. coli* and then evaluated for autophosphorylation of the EGFR in A431 cells.

single-cell analysis and isolation system to promptly identify six novel EGFR agonists that are active in A431 cells.

A cell wall is one of the major differences between yeast and mammalian cells. The thickness and pore size of the yeast cell wall are 50 ~ 200 nm[27] and about 0.89 nm, respectively[28]. Because the size of the extracellular domain of the EGFR and the Stokes radius of EGF are about 11 nm[29] and 3.2 nm[30], respectively, extracellular proteinous ligands cannot reach the EGFR buried in the cell wall, and ligands expressed in the vicinity of the yeast plasma membrane can interact with the EGFR. Thus, each yeast cell concurrently displaying the receptor and ligand candidates can work as 'an independent and autonomous test tube', allowing us to analyze a ligand-receptor interaction at a single cell level without exogenous interference. By displaying ligands on the yeast cell surface, molecules accumulate in the periplasm and cell wall[31]. Assuming that yeast cells are spheres of a 5.5 μm average diameter (n = 40), and the average thickness of the cell wall is 125 nm[27], the volume of periplasmic and cell wall fractions is calculated as about 1.135×10^{-11} ml. Because the maximal number of small molecules displayed on the yeast cell surface is estimated to be about 10^6 per yeast cell[32,33], the maximal concentration of cell wall-anchored EGF is estimated at 146 μM, which implies that a 1.2×10^5-fold of the EC_{50} of EGF (1.2 nM) to activate the EGFR in mammalian cells[34]. High concentrations of ligands on the yeast cell surface facilitate the identification of ligands, even if their agonistic activities are very low.

When yeast cells co-expressing the EGFR and HLH peptide library were established, we initially tried to isolate yeast cells with high fluorescence by fluorescence-activated cell sorting (FACS). Because conventional FACS systems only collect positive cells with a proportion of more than 0.1%[19,35], we could not isolate positive clones (up to 100) from a peptide library of more than 1×10^6 by FACS. To address this issue, we used an automated single-cell analysis and isolation system that manipulates single cells arrayed on a chip with 250,000 microchambers. Consequently, 83 positive cells were isolated from about 3.2×10^6 independent clones, indicating that the automated single-cell analysis and isolation system can manipulate positive cells at a proportion of less than 0.0026%. In principle, the system can isolate yeast cells with the highest fluorescence from a peptide library of more than 10^6, which is nearly impossible by FACS.

A random peptide library with a flexible structure often weakly interacts with target molecules in an induced-fit manner[36], leading to identification of false-positive molecules. Accordingly, we employed a conformationally constrained HLH peptide library for EGFR agonist screening. DNA sequence analyses revealed several independent clones encoding identical amino acid sequences (Supplementary Table S1), and about 85% of positive clones (11/13) could activate the EGFR in A431 cells, which strongly suggests that the HLH peptide library is reliable for drug screening. Previous studies with EGF

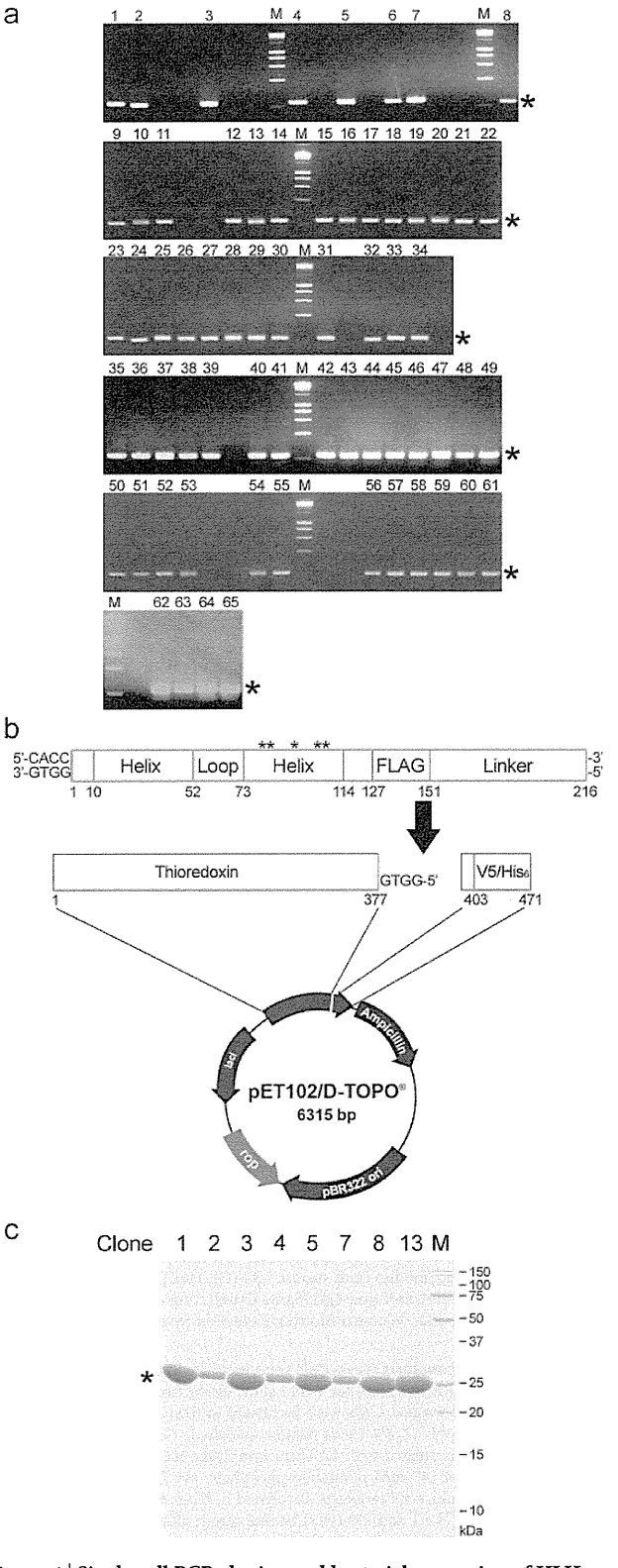

Figure 4 | Single-cell PCR cloning and bacterial expression of HLH proteins. (a) Single-cell PCR. PCR products obtained by single-cell PCR were subjected to agarose gel electrophoresis. Numbers indicate clones amplified successfully (65 clones/83 lanes). M, DNA marker. Asterisks indicate the position of target bands. (b) Directional TOPO cloning. The cDNA fragments amplified by single cell PCR (216 bp) were extracted from agarose gel, and then inserted into pET102 directional TOPO vector for the bacterial expression. Loop encodes hepta-glycine. Linker encodes N-terminal 20 amino acids of FLO42. Asterisks indicate the position of identical codon. (c) Purification of HLH proteins. HLH proteins expressed as an N-terminal thioredoxin-fused and C-terminal hexahistidine-tagged form in *Escherichia coli* BL21 (DE3) and purified with cobalt-chelating column. The purity was checked by CBB staining. Numbers indicate the clone number. M, protein marker. Asterisk indicates the position of target band.

mutants have revealed that some amino acid residues in EGF (Tyr-13, Leu-15, His-16, Arg-41, Gln-43 and Lue-47)[37,38] together with Gly-12[39] play a key role for EGFR binding and/or mitogenicity in mammalian cells (Supplementary Table S3). Furthermore, by using a fluorescence-labeled EGFR extracellular domain as a probe for EGF mutants displayed on the yeast cell surface, Cochran *et al.*[40] and Lahti *et al.*[41] have identified and analyzed various EGFR agonists, in which mutant 114, 28 and 123 possess over 30-fold affinity to EGFR compared with wild-type EGF[40,41]. When comparing the amino acid sequences among the previously reported EGF mutants and the HLH peptides harboring EGFR agonistic activity (*see* Supplementary Table S3), the HLH peptides are fundamentally different from these EGF mutants not only in primary structure but also secondary structure. Thus, the biological function of each amino acid contained in the HLH and EGF mutants could not be completely compared. However, while some high affinity EGF mutants have been found to contain additional 1 ~ 4 Pro[40], this amino acid residue was found in the identified HLH peptides at high frequency (4 of 6 agonistic HLH peptides; *i.e.*, clone 2, 7, 8, 13). Since Pro is known to be α-helix breaker, the C-terminal α-helix of HLH peptides was presumably somewhat too straight to bind to EGFR structurally. On the other hand, HLH clone 4, which contains two Pro, did not show the EGFR agonistic activity, suggesting that the C-terminal α-helix of HLH peptides was essentially required to activate EGFR but should harbor a shorter or bent helix structure for more efficient EGFR activation. All EGFR agonist candidates selected by yeast-based screening were considered to possess high activity also in mammalian cells. Unexpectedly, two proteins (derived from clones 1 and 4) showed no agonistic activity, and also 11 proteins showed low activity in A431 cells. This was probably caused by the differences of cellular conditions around EGFR between yeast cells and A431 cells and/or by insufficient contributions from randomized 5 amino acid residues located to C-terminal α-helix of the HLH peptides to bind to EGFR. If the screening of EGFR agonists with new peptide libraries (*e.g.*, HLH scaffold harboring >6 randomized amino acid residues, new scaffold optimized for EGFR) is performed, new peptides with strong EGFR agonistic activity could be identified. Taken together, it is still worth performing the agonist screening in yeast cells for identifying lead compounds with novel structure in a high-throughput manner. Furthermore, as reported by Fujii *et al.*[18], this library is suitable for extracting pharmacophores to design small chemical compounds by molecular dynamics simulation.

A single cell-based high-throughput drug screening system using yeast cell surface engineering to facilitate prompt *de novo* screening of lead compounds for rational drug design may accelerate the introduction of yeast technology to conventional mammalian cell-based drug discovery.

Methods

Plasmids. A DNA fragment encoding the yeast α-factor-prepro region (MFα1prepro, N-terminal 89 amino acids of the MFα1 precursor), N-terminal HA-tagged human EGF (HA-EGF) and yeast cell wall-anchored peptide FLO42 (C-terminal 42 amino acids of FLO1) was inserted under the control of the *GAL1* promoter into pYES2 (*URA3*, Invitrogen, Carlsbad, CA, USA) (pYES2-MFα1prepro-HA-EGF-FLO42, *see* Figure 1b). By replacing *EGF*-coding region with human *IL5* gene, pYES2-MFα1prepro-HA-IL5-FLO42 was constructed for the expression of non EGFR-related ligand. A DNA fragment encoding the SUC2 signal peptide (25 amino acids), human EGFR (mature form, Leu-25 to Ala-1210 of the EGFR precursor, GenBank accession No. NM_005228.3) and C-terminal V5-tagged EGFR was inserted under

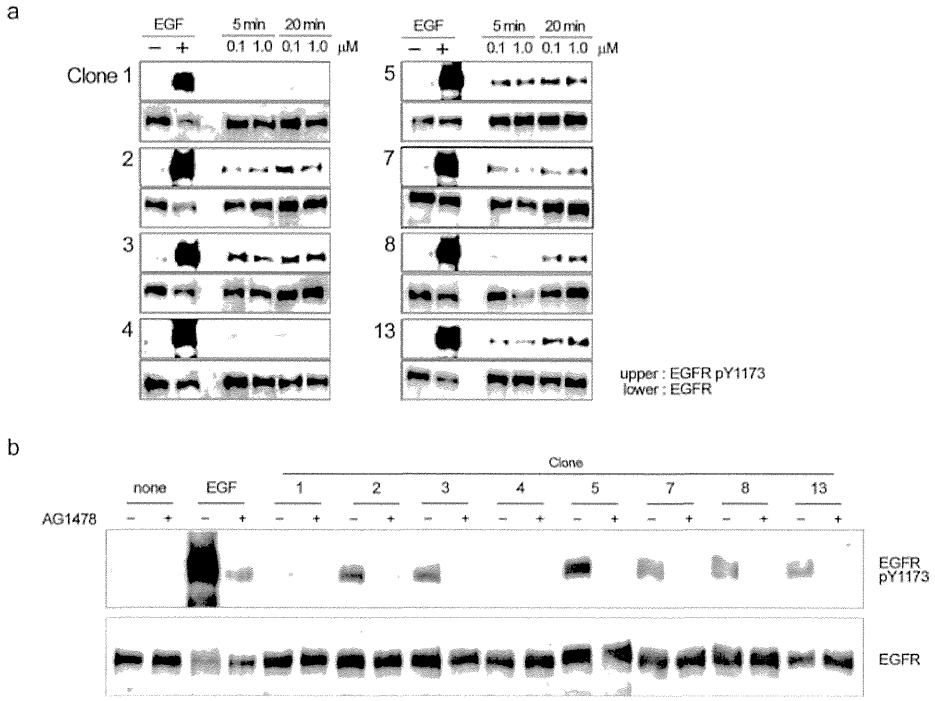

Figure 5 | Induction of EGFR autophosphorylation in A431 cells by EGFR agonist candidates. (a) After treatment with 0.1 and 1.0 μM bacterially expressed HLH peptides (8 species, clones 2 ~ 17) for 5 and 20 min, A431 cell lysates were subjected to western blotting with anti-EGFR and anti-EGFR pY1173 antibodies. As a positive control, 1.5 nM EGF was used. (b) After 30-min treatment with 200 nM tyrphostin AG1478, A431 cells were treated with 2.0 μM HLH peptides for 20 min, lysed and subjected to western blotting with anti-EGFR and anti-EGFR pY-1173 antibodies. As a positive control, 1.5 nM EGF was used.

the control of the *GAL1* promoter into pYES3 (*TRP1*, Invitrogen) (pYES3-SUC-EGFR-V5, *see* Figure 1b).

As a conformationally constrained peptide library, the DNA fragment encoding MFα1prepro, an intramolecular anti-parallel HLH peptide with a C-terminal FLAG tag and FLO42 was inserted under the control of the *GAL1* promoter into pYES2 (pYES2-MFα1prepro-HLH-FLAG-FLO42). Briefly, primary PCR was carried out using 5′-CGC CAA GCT TGG GCG GAG CTC GCA GCT CTG GAA ATG GAA CTG GCG GCA CTC GAA GGT GGC GGC GGT GGT GGC GGC AAG CTG-3′ and 5′-T CCG CTC GAG TTT ATC ATC ATC ATC TTT ATA ATC GGA GCC TCC ACC AGC TTT CAA MNN MNN TAG CTT MNN TTT CAA MNN MNN CAG CTT GCC GCC ACC ACC-3′, in which N represents A, T, G or C, and M represents A or C. The DNA fragment encoding randomized HLH-FLAG moiety was further amplified by using 5′-CGC CAA GCT TGG GCG GAG-3′ and 5′-TCC GCT CGA GTT TAT CAT CAT CAT CTT TAT-3′, treated with *Hind* III and *Xho* I, and then inserted into pYES2-MFα1prepro-FLO42 vector. The HLH peptide contained randomized sequences of five amino acids on the solvent-accessible surface of the second helix.

To examine homo-oligomerization of the EGFR, the DNA fragment of the human EGFR (mature form) was inserted under the control of the *ADH1* promoter of pPR3-SUC (*TRP1*, Mo Bi Tech, Göttingen, Germany) to express an N-terminal SUC2 signal peptide-fused and C-terminal Nub (N-terminal half of human ub)-fused form (pPR3-SUC-EGFR), and the same DNA fragment was inserted under the control of the *CYC1* promoter into pBT3-SUC (*LEU2*, Mo Bi Tech) to express an N-terminal SUC2 signal peptide-fused and C-terminal Cub (C-terminal half of human ub)-LexA (DNA-binding domain)-VP16 (transactivating domain)-fused form (pBT3-SUC-EGFR).

To examine interactions of the EGFR with Grb2 and Shc1, the DNA fragment encoding MFα1prepro and N-terminal FLAG-tagged EGFR was inserted under the control of the *GAL1* promoter of pGMH20 (*HIS3*, RIKEN Bioresource Center, Ibaraki, Japan) (pGMH20-MFα1prepro-FLAG-EGFR). Human *Grb2* cDNA (NM_002086.4) and human *Shc1* cDNA (NM_183001.3) were inserted under the control of the *ADH1* promoter of the pSos plasmid (Stratagene, La Jolla, CA, USA) to express an N-terminal Sos (N-terminal 1063 amino acids of Sos)-fused form of Grb2 (pSos-Grb2) and Shc1 (pSos-Shc1), respectively.

Yeast strains. *S. cerevisiae* BJ5464 (MATα ura3-52 his3-200 trp1 leu2-1 pep4::HIS3 prb1Δ1.6R can1 Gal^+) was obtained from the Yeast Genetic Resource Center (Osaka, Japan). *S. cerevisiae* cdc25h (MATa ura3-52 his3-200 trp1-901 leu2-3,112 ade2-101 lys2-801 cdc25-2 Gal^+) and NMY51 (MATa his3-200 trp1-901 leu2-3,112 ade2 ura3::$(lexAop)_8$-lacZ LYS2::$(lexAop)_4$-HIS3 $(lexAop)_8$-ADE2 GAL4) were purchased from Stratagene and Mo Bi Tech, respectively. Manipulation of yeast cells was performed according to the yeast protocol handbook (Clontech).

Western blotting. Yeast cells were incubated with SD medium containing 20 mM HEPES (pH 7.0) for 1 h to allow interaction between EGF and the EGFR on the yeast cell surface. When using tyrphostin AG1478 (*N*-(3-chlorophenyl)-6,7-dimethoxy-4-quinazolinamine) (Cell Signaling Technology, Beverly, MA, USA), cells were treated with the reagent at 1 μM for 30 min before lysis. Yeast cells were suspended in a lysis buffer (50 mM Tris-HCl, pH 7.2, 150 mM NaCl, 1 mM EGTA, 1% (v/v) Triton X-100, 2 mM dithiothreitol and 1 tablet per 10 ml Complete™ protease inhibitor cocktail (Roche, Basel, Switzerland), frozen in liquid nitrogen and then disrupted with vigorous shaking in an automatic homogenizer (Automill™; Tokken, Chiba, Japan). After centrifugation, the supernatant was collected as the cytosolic fraction. The cell-wall fraction was extracted from cell debris with 0.5% (w/v) SDS and 1% (v/v) 2-mercaptomethanol[42]. Each fraction was subjected to SDS-PAGE followed by western blotting with a horseradish peroxidase (HRP)-conjugated anti-HA antibody (clone 12CA5, Roche), an HRP-conjugated anti-V5 antibody (clone V5–10, Sigma-Aldrich, St Louis, MO, USA), anti-EGFR pY-1068 mouse monoclonal antibody (clone 15A2, nanoTools, Teningen, Germany), anti-EGFR pY-1148 rabbit polyclonal antibody (Novus Biologicals, Littleton, CO, USA), anti-EGFR pY-1173 goat polyclonal antibody (Santa Cruz Biotechnology, Santa Cruz, CA, USA) and appropriate HRP-conjugated secondary antibodies (anti-mouse IgG (GE Healthcare, St. Giles), anti-rabbit IgG (GE Healthcare), anti-goat IgG (Santa Cruz)). Immunoreactive bands were visualized with an ECL Plus Western Blotting Detection System (GE Healthcare).

Immunocytochemical analysis. Yeast cells were incubated with SD medium containing 20 mM HEPES (pH 7.0) for 1 h to allow interaction between EGF and the EGFR on the yeast cell surface. Cells were incubated in fixation buffer (40 mM potassium phosphate, pH 7.2, 4% (w/v) paraformaldehyde (PFA) at room temperature for 30 min, treated with 12 U/ml zymolyase 100 T (Seikagaku, Tokyo, Japan) in sorbitol buffer (40 mM potassium phosphate, pH 7.2, 1.2 M sorbitol and 0.5 mM $MgCl_2$) to produce spheroplasts, incubated in blocking buffer (10 mM Tris-HCl, pH 7.2, 150 mM NaCl and 2% (w/v) bovine serum albumin (BSA) and then labeled with appropriate primary antibodies at room temperature for 1 h. To detect HA-EGF-FLO42 and HA-IL5-FLO42, intact cells were used instead of spheroplasts. Labeled cells were washed with TBS (10 mM Tris-HCl, pH 7.2 and 150 mM NaCl), incubated in blocking buffer containing Alexa Fluor 488-labeled anti-IgG (Invitrogen) at room temperature for 30 min, washed with TBS and then analyzed with a FLUOVIEW FV1000 confocal laser scanning microscope (Olympus, Tokyo, Japan) and FACSCanto™ II flow cytometer (BD Biosciences, San Jose, CA, USA). Antibodies used were as follows: anti-HA (clone 12CA5), anti-V5 (clone V5005, Nacalai, Kyoto, Japan), anti-EGFR phosphotyrosine-1068 (pY-1068) (clone 15A2, nanoTools, Teningen, Germany), anti-EGFR pY-1148 (Novus Biologicals, Littleton, CO, USA) and anti-EGFR pY-1173 (Santa Cruz Biotechnology, Santa Cruz, CA, USA).

Split-ub membrane two-hybrid assay. *S. cerevisiae* NMY51 harboring pPR3-SUC-EGFR (pray), pBT3-SUC-EGFR (bait) and either pYES2-MFα1prepro-HA-EGF-FLO42 (ligand) or pYES2-MFα1prepro-FLO42 (control) were plated on a His-depleted SD plate or an X-Gal-containing SD plate and incubated at 30°C for 8 days.

Complementation assay with the CDC25^{ts} strain. *S. cerevisiae* cdc25h harboring pGMH20-MFα1prepro-FLAG-EGFR, either pSos-Grb2 or pSos-Shc1 and either pYES2-MFα1prepro-HA-EGF-FLO42 (ligand) or pYES2-MFα1prepro-FLO42 (control) were plated on an SD plate and incubated at 25 or 37°C for 7 days.

***De novo* agonist screening with an automated single-cell analysis and isolation system.** *S. cerevisiae* BJ5464 cells harboring pYES2-MFα1prepro-HLH-FLAG-FLO42 and pYES3-SUC-EGFR-V5 were incubated with SD medium containing 20 mM HEPES (pH 7.0) for 1 h, fixed with PFA, treated with zymolyase, blocked with BSA and then stained with an anti-EGFR pY1173 antibody. Approximately 2.5×10^5 fixed spheroplasts in 1 ml PBS were individually placed into the microchambers (10 μm diameter, 30 μm well-to-well pitch and 10 μm well depth) of a cell array chip (256,000 wells; 20 × 20 wells/subarea; 20 × 32 subareas/chip on a 1.39 × 2.23 cm^2 chip) by brief centrifugation (7 × *g* at room temperature for 1 min, three times) and then analyzed with the automated single-cell analysis and isolation system (As One corp., Osaka, Japan). Each cell with high fluorescence was collected by the automated single-cell analysis and isolation system in descending order of fluorescent intensity as described previously[19]. Briefly, microchambers containing no or more than 2 fluorescent spheroplasts were excluded from further analyses. A histogram together with a list of correlations between the position and fluorescent intensity of each spheroplast was generated. Target spheroplasts could be virtually marked in descending order of fluorescent intensity. Spheroplasts of interest were automatically collected with a glass capillary attached to the micromanipulator of the automated single-cell analysis and isolation system, which were optimized not to pick up the adjacent non-target spheroplasts and confirmed by elimination of fluorescence in the target microchamber automatically. Upon failure, the system automatically repeated the collection process. Each spheroplast was transferred and released into the assigned well in 96-well PCR plates. The reciprocal movement of the glass capillary required 15 s for each spheroplast. After repeating the procedure 20 times, 83 spheroplasts as positive clones isolated from about 3.2×10^6 independent clones were moved to a 96 well PCR plate and then subjected to single cell-based PCR. Primary PCR was carried out using 5′-GCC TTA TTT CTG GGG TAA TTA ATC AGC G-3′, 5′-ACC TAG ACT TCA GGT TGT CTA ACT CCT TCC-3′ and KOD-Plus- (TOYOBO, Osaka, Japan) to amplify the DNA fragment encoding the *GAL1* promoter, MFα1prepro-HLH-FLAG-FLO42 and *CYC1* terminator. The thermal cycling of the primary PCR was pre-heating at 94°C for 5 min; 12 cycles of denaturing at 94°C for 1 min; annealing from 73°C to 61°C (−1°C/cycle) for 20 sec; extension at 68°C for 90 sec; followed by 45 cycles of denaturing at 94°C for 1 min; annealing at 64°C for 30 sec; extension at 68°C for 90 sec and final extension at 68°C for 7 min. The secondary PCR was carried out using 5′-CAC CCA AGC TTG GGC GGA GCT CGC AGC TCT-3′, 5′-GGC ACT GCC AGC ATA CGT TGA AAT-3′ and KOD-Plus- to amplify the DNA fragment encoding HLH-FLAG and the N-terminal 20 amino acids of FLO42. The thermal cycling of the secondary PCR was pre-heating at 94°C for 2 min; 12 cycles of denaturing at 94°C for 1 min; annealing from 77°C to 63°C (−1°C/cycle) for 20 sec; extension at 68°C for 15 sec; followed by 45 cycles of denaturing at 94°C for 1 min; annealing at 66°C for 30 sec; extension at 68°C for 15 sec and final extension at 68°C for 7 min. The amplified DNA fragments were inserted under the control of the T7 promoter in the pET102/D-TOPO vector (Invitrogen) (pET102-HLH-FLAG).

Bacterial expression of EGFR agonist candidates. *E. coli* BL21 (DE3) harboring pET102-HLH-FLAG was cultured in an Overnight Express Autoinduction System (Merck, Darmstadt, Germany). N-terminal thioredoxin (TRX)-fused and C-terminal His6-tagged forms of HLH-FLAG were purified by the BD TALON™ HT 96-Well Purification System (BD) according to the manufacture's protocol. Homogeneity of TRX-HLH-FLAG-His6 protein was confirmed by SDS-PAGE followed by Coomassie brilliant blue R-250 staining.

Autophosphorylation assay in A431 cells. Human squamous carcinoma A431 cells (approximately 5×10^4 cells) cultured on a 3.5 cm dish were incubated in serum-free medium for 16 h and then treated with 0.1, 1.0, or 2.0 μM TRX-HLH-FLAG-His6 proteins for 5 and 20 min. As a positive control, 1.5 nM recombinant human EGF (PEPROTECH, Rocky Hill, NJ, USA) was used. When using tyrphostin AG1478, cells were treated with the reagent at 200 nM for 30 min before ligand (*i.e.*, EGF, HLH) treatment. Cells were lysed with lysis buffer (50 mM Tris-HCl, pH 7.2, 150 mM NaCl, 1 mM EGTA, 1% Triton X-100, 1 mM Na_3VO_4, 1% (v/v) phosphatase inhibitor cocktail I (SIGMA) and 1 tablet/50 ml Complete™ (Roche), mixed with 1 × Laemmli's sample buffer and then boiled for 15 min. Samples were analyzed by western blotting using anti-EGFR (Rockland, Gilbertsville, PA, USA) and anti-EGFR pY-1173 antibodies.

1. Smith, C. & Teitler, M. Beta-blocker selectivity at cloned human beta 1- and beta 2-adrenergic receptors. *Cardiovasc. Drugs Ther.* **13**, 123–126 (1999).
2. Lazou, A., Sugden, P. H. & Clerk, A. Activation of mitogen-activated protein kinases (p38-MAPKs, SAPKs/JNKs and ERKs) by the G-protein-coupled receptor agonist phenylephrine in the perfused rat heart. *Biochem. J.* **332**, 459–465 (1998).
3. Sirotnak, F. M., Zakowski, M. F., Miller, V. A., Scher, H. I. & Kris, M. G. Efficacy of cytotoxic agents against human tumor xenografts is markedly enhanced by coadministration of ZD1839 (Iressa), an inhibitor of EGFR tyrosine kinase. *Clin. Cancer Res.* **6**, 4885–4892 (2000).
4. Slamon, D. J. *et al.* Use of chemotherapy plus a monoclonal antibody against HER2 for metastatic breast cancer that overexpresses HER2. *N. Engl. J. Med.* **344**, 783–792 (2001).
5. Costa-Pereira, A. P. *et al.* Mutational switch of an IL-6 response to an interferon-gamma-like response. *Proc. Natl. Acad. Sci. USA* **99**, 8043–8047 (2002).
6. Velloso, L. A. *et al.* Cross-talk between the insulin and angiotensin signaling systems. *Proc. Natl. Acad. Sci. USA* **93**, 12490–12495 (1996).
7. Suzuki, A. *et al.* CIS3/SOCS3/SSI3 plays a negative regulatory role in STAT3 activation and intestinal inflammation. *J. Exp. Med.* **193**, 471–481 (2001).
8. Antonio, C. N., Grazia, P. M., Marialessandra, C., Francesco, B. & Roberto, P. Receptor-drug interaction: europium employment for studying the biochemical pathway of g-protein-coupled receptor activation. *Met. Based Drugs* **2007**, 12635 (2007).
9. Luque, R. M. *et al.* Differential contribution of nitric oxide and cGMP to the stimulatory effects of growth hormone-releasing hormone and low-concentration somatostatin on growth hormone release from somatotrophs. *J. Neuroendocrinol.* **17**, 577–582 (2005).
10. Finch, E. A., Turner, T. J. & Goldin, S. M. Calcium as a coagonist of inositol 1,4,5-trisphosphate-induced calcium release. *Science* **252**, 443–446 (1991).
11. Naider, F. & Becker, J. M. The alpha-factor mating pheromone of *Saccharomyces cerevisiae*: a model for studying the interaction of peptide hormones and G protein-coupled receptors. *Peptides* **25**, 1441–1463 (2004).
12. Minic, J., Sautel, M., Salesse, R. & Pajot-Augy, E. Yeast system as a screening tool for pharmacological assessment of g protein coupled receptors. *Curr. Med. Chem.* **12**, 961–969 (2005).
13. Miret, J. J., Rakhilina, L., Silverman, L. & Oehlen, B. Functional expression of heteromeric calcitonin gene-related peptide and adrenomedullin receptors in yeast. *J. Biol. Chem.* **277**, 6881–6887 (2002).
14. Floyd, D. H. *et al.* C5a receptor oligomerization. II. Fluorescence resonance energy transfer studies of a human G protein-coupled receptor expressed in yeast. *J. Biol. Chem.* **278**, 35354–35361 (2003).
15. Klein, C. *et al.* Identification of surrogate agonists for the human FPRL-1 receptor by autocrine selection in yeast. *Nat. Biotechnol.* **16**, 1334–1337 (1998).
16. Manning, G., Plowman, G. D., Hunter, T. & Sudarsanam, S. Evolution of protein kinase signaling from yeast to man. *Trends Biochem. Sci.* **27**, 514–520 (2002).
17. Busti, S., Sacco, E., Martegani, E. & Vanoni, M. Functional coupling of the mammalian EGF receptor to the Ras/cAMP pathway in the yeast *Saccharomyces cerevisiae*. *Curr. Genet.* **53**, 153–162 (2008).
18. El-Haggar, R. *et al.* Molecular design of small organic molecules based on structural information for a conformationally constrained peptide that binds to G-CSF receptor. *Bioorg. Med. Chem. Lett.* **20**, 1169–1172 (2010).
19. Yoshimoto, N. *et al.* An automated system for high-throughput single cell-based breeding. *Sci. Rep.* **3**, 1191 (2013).
20. Emr, S. D., Schekman, R., Flessel, M. C. & Thorner, J. An MF alpha 1-SUC2 (alpha-factor-invertase) gene fusion for study of protein localization and gene expression in yeast. *Proc. Natl. Acad. Sci. USA* **80**, 7080–7084 (1983).
21. Sato, N. *et al.* Long anchor using Flo1 protein enhances reactivity of cell surface-displayed glucoamylase to polymer substrates. *Appl. Microbiol. Biotechnol.* **60**, 469–474 (2002).
22. Bielefeld, M. & Hollenberg, C. P. Bacterial beta-lactamase is efficiently secreted in *Saccharomyces cerevisiae* under control of the invertase signal sequence. *Curr. Genet.* **21**, 265–268 (1992).
23. Johns, T. G. *et al.* Antitumor efficacy of cytotoxic drugs and the monoclonal antibody 806 is enhanced by the EGF receptor inhibitor AG1478. *Proc. Natl. Acad. Sci. USA* **100**, 15871–15876 (2003).
24. Ferguson, K. M. *et al.* EGF activates its receptor by removing interactions that autoinhibit ectodomain dimerization. *Mol. Cell* **11**, 507–517 (2003).
25. Stagljar, I., Korostensky, C., Johnsson, N. & te Heesen, S. A genetic system based on split-ubiquitin for the analysis of interactions between membrane proteins *in vivo*. *Proc. Natl. Acad. Sci. USA* **95**, 5187–5192 (1998).
26. Petitjean, A., Hilger, F. & Tatchell, K. Comparison of thermosensitive alleles of the *CDC25* gene involved in the cAMP metabolism of *Saccharomyces cerevisiae*. *Genetics* **124**, 797–806 (1990).
27. Linnemans, W. A., Boer, P. & Elbers, P. F. Localization of acid phosphatase in *Saccharomyces cerevisiae*: a clue to cell wall formation. *J. Bacteriol.* **131**, 638–644 (1977).
28. De Nobel, J. G. *et al.* Cyclic variations in the permeability of the cell wall of *Saccharomyces cerevisiae*. *Yeast* **7**, 589–598 (1991).
29. Lemmon, M. A. *et al.* Two EGF molecules contribute additively to stabilization of the EGFR dimer. *EMBO J.* **16**, 281–294 (1997).
30. Nexø, E., Jørgensen, P. E., Thim, L. & Roepstorff, P. Purification and characterization of a low and a high molecular weight form of epidermal growth factor from rat urine. *Biochim. Biophys. Acta* **1037**, 388–393 (1990).
31. Jin, Y. L. & Speers, R. A. Flocculation of *Saccharomyces cerevisiae*. *Food Res. Int.* **31**, 421–440 (1998).

32. Ueda, M. & Tanaka, A. Genetic immobilization of proteins on the yeast cell surface. *Biotechnol. Adv.* **18**, 121–140 (2000).
33. Takayama, K. *et al.* Surface display of organophosphorus hydrolase on *Saccharomyces cerevisiae*. *Biotechnol. Prog.* **22**, 939–943 (2006).
34. Gilmore, J. L., Gallo, R. M. & Riese, D. J. 2nd. The epidermal growth factor receptor (EGFR)-S442F mutant displays increased affinity for neuregulin-2beta and agonist-independent coupling with downstream signalling events. *Biochem. J.* **396**, 79–88 (2006).
35. Yamamura, S. *et al.* Single-cell microarray for analyzing cellular response. *Anal. Chem.* **77**, 8050–8056 (2005).
36. Rini, J. M., Schulze-Gahmen, U. & Wilson, I. A. Structural evidence for induced fit as a mechanism for antibody-antigen recognition. *Science* **255**, 959–965 (1992).
37. Campbell, I. D., Cooke, R. M., Baron, M., Harvey, T. S. & Tappin, M. J. The solution structures of epidermal growth factor and transforming growth factor alpha. *Prog. Growth Factor Res.* **1**, 13–22 (1989).
38. Souriau, C., Gracy, J., Chiche, L. & Weill, M. Direct selection of EGF mutants displayed on filamentous phage using cells overexpressing EGF receptor. *Biol. Chem.* **380**, 451–458 (1999).
39. Mullenbach, G. T. *et al.* Modification of a receptor-binding surface of epidermal growth factor (EGF): analogs with enhanced receptor affinity at low pH or at neutrality. *Protein Eng.* **11**, 473–480 (1998).
40. Cochran, J. R., Kim, Y. S., Lippow, S. M., Rao, B. & Wittrup, K. D. Improved mutants from directed evolution are biased to orthologous substitutions. *Protein Eng. Des. Sel.* **19**, 245–253 (2006).
41. Lahti, J. L. *et al.* Engineered epidermal growth factor mutants with faster binding on-rates correlate with enhanced receptor activation. *FEBS Lett.* **585**, 1135–1159 (2011).
42. Schreuder, M. P., Brekelmans, S., van den Ende, H. & Klis, F. M. Targeting of a heterologous protein to the cell wall of *Saccharomyces cerevisiae*. *Yeast* **9**, 399–409 (1993).

Acknowledgments

We are grateful to Prof. Hidekatsu Iha (Oita University) for pGMH20 and pGMT20 vectors. This study was supported in part by Adaptable & Seamless Technology Transfer Program through Target-driven R&D (A-STEP) by the Japan Science and Technology Agency (JST) (AS231Z04687F to N.Y., AS2311699F to S.K.), the Program for Promotion of Basic and Applied Researches for Innovations in Bio-oriented Industry (H22-7, BRAIN to S.K.), a Grant-in-Aid for Scientific Research (A) (25242043 to S.K.), the Health Labor Sciences Research Grant from the Ministry of Health Labor and Welfare (to S.K.), and the As One Corporation (to S.K.). We thank Jun Ishii (Kobe University), Ken-ichi Kimura and Xu Jie (Furukawa), Masato Fujihashi and Masaya Kurokawa (STARLITE), and Masahiro Matsushita, Kenji Uemukai, and Tohru Kaneno (As One).

Author contributions

N.Y., K.Tatematsu, I.F., A.K., K.Tanizawa and S.K. designed research; N.Y., K.Tatematsu, M.I., T.N. and A.D.M. performed research; N.Y., K.Tatematsu and S.K. analyzed data; and N.Y. and S.K. wrote the paper.

Additional information

Supplementary information accompanies this paper at http://www.nature.com/scientificreports

Competing financial interests: The authors declare no competing financial interests.

How to cite this article: Yoshimoto, N. *et al.* High-throughput *de novo* screening of receptor agonists with an automated single-cell analysis and isolation system. *Sci. Rep.* **4**, 4242; DOI:10.1038/srep04242 (2014).

High-throughput *de novo* screening of receptor agonists with an automated single-cell analysis and isolation system

Author names

Nobuo Yoshimoto[1,*], Kenji Tatematsu[2], Masumi Iijima[1], Tomoaki Niimi[1], Andrés D. Maturana[1], Ikuo Fujii[3], Akihiko Kondo[4], Katsuyuki Tanizawa[2] & Shun'ichi Kuroda[1,*]

Affiliations

[1] Graduate School of Bioagricultural Sciences, Nagoya University, Furo-cho, Chikusa-ku, Nagoya, Aichi 464-8601, Japan;

[2] The Institute of Scientific and Industrial Research, Osaka University, Mihogaoka, Ibaraki, Osaka 567-0047, Japan;

[3] Graduate School of Science, Osaka Prefecture University, Gakuen-cho, Naka-ku, Sakai, Osaka 599-8570, Japan;

[4] Graduate School of Science and Technology, Kobe University, Rokkodai-cho, Nada-ku, Kobe, Hyogo 657-8501, Japan.

Correspondence and requests for materials should be addressed to N. Y. (n-yosi44@agr.nagoya-u.ac.jp) & S. K. (skuroda@agr.nagoya-u.ac.jp).

Supplementary Information

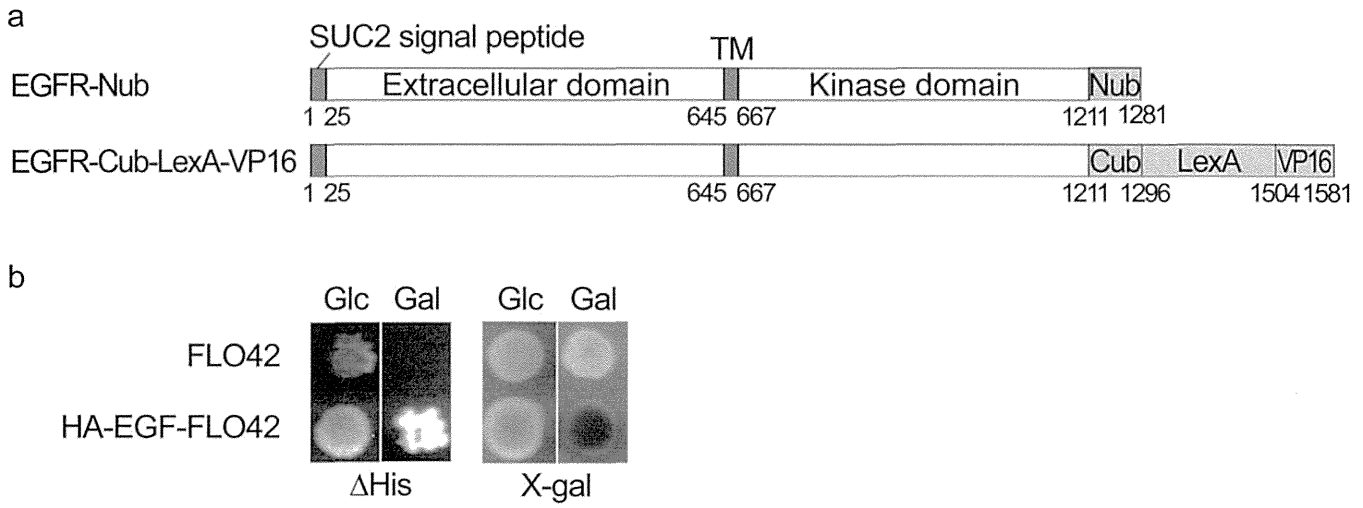

Supplementary Figure S1. EGF-dependent homo-oligomerization of the EGFR in the yeast plasma membrane. (a) Molecular organizations of EGFRs in a split-ub assay. *TM*, transmembrane domain; *Nub*, N-terminal half of ub; *Cub*, C-terminal half of ub; *LexA*, DNA-binding domain of LexA; *VP16*, transcription-activating domain of VP16. **(b)** Split-ub assay. The yeast NMY51 strain co-expressing EGFR-Nub, EGFR-Cub-LexA-VP16 and either FLO42 or HA-EGF-FLO42 was spotted onto an SD plate (pH 7) containing glucose (*Glc*, for repression of *GAL1* promoter) or galactose (*Gal*, for induction of *GAL1* promoter). *ΔHis*, histidine-depleted SD medium; *X-gal*, X-gal-containing SD medium.

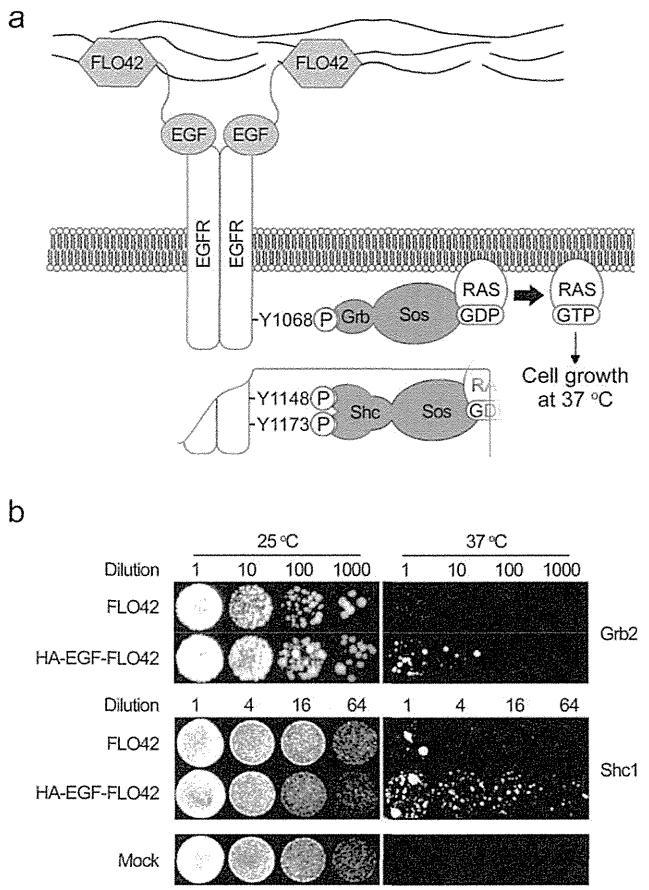

Supplementary Figure S2. Functional interaction of the EGFR with Grb2 and Shc1 in yeast cells. (a) Schematic drawing of the EGF signaling pathway reconstituted in yeast cells. N-terminal human Sos-fused forms of human adaptor proteins, Grb2 (*Grb*) and Shc1 (*Shc*), interact with phospho-EGFR in yeast cells. The membrane-recruited Sos is a guanine nucleotide-exchanging factor for human Ras, which converts yeast RAS from the GDP (inactive) form to the GTP (active) form and complements thermo-sensitive $CDC25^{TS}$ in the yeast cdc25h strain, thereby allowing yeast cells to grow at 37 °C. **(b)** Complementation of thermo-sensitivity of the yeast cdc25h strain by EGF-dependent activation of the RAS signaling pathway. The yeast cdc25h strain co-expressing EGFR-V5 and either FLO42 or HA-EGF-FLO42 was spotted onto an SD plate and then incubated at 25 °C or 37 °C. *Grb2* and *Shc1* indicate the cdc25h strains expressing Sos-Grb2 and Sos-Shc1, respectively.

Supplementary Table S1. Nucleotide sequences of secondary helix-cording region for EGFR agonist candidates

Clone no.	nucleotide sequences*
1	AAGCTGTATTCGTTGAAAATGAAGCTACATAAGTTGAAAGCT
2	AAGCTGGATCCGTTGAAAATTAAGCTAGAGTCGTTGAAAGCT
3	AAGCTGTCTTCGTTGAAAGCTAAGCTATCTCATTTGAAAGCT
4	AAGCTGCCTAAGTTGAAACATAAGCTACCGACGTTGAAAGCT
5	AAGCTGAATCGTTTGAAACATAAGCTATCGTTTTTGAAAGCT
6	AAACTGGATCCGTTGAAAATTAAGCTAGAGTCGTTGAAAGCT
7	AAGCTGATTTGTTTGAAACATAAGCTAACGCCTTTGAAAGCT
8	AAGCTGACTCCTTTGAAAAAGAAGCTAACTGCTTTGAAAGCT
9	AAGCTGGATCCTTTGAAAATTAAGCTAGAGTCGTTGAAAGCT
10	AAGCTGGATCCGTTGAAAATTAAGCTAGAGTCGTTGAAAGCT
11	AAGCTGACTCCTTTGAAAAAGAAGCTAACTGCTTTGAAAGCT
12	AAGCTGACTCCTTTGAAAAAGAAGCTAACTGCTTTGAAAGCT
13	AAGCTGCCGCTTTTGAAATCTAAGCTATTGTCTTTGAAAGCT

* Identified nucleic acids are shown in red.

Supplementary Table S2. Amino acid sequences of EGFR agonist candidates

Clone no.	Amino acid sequences*	Notes
1	KLYSLKMKLHKLKA	No agonistic activity
2	KLDPLKIKLESLKA	Identical to clones 6, 9 and 10
3	KLSSLKAKLSHLKA	
4	KLPKLKHKLPTLKA	No agonistic activity
5	KLNRLKHKLSFLKA	
7	KLICLKHKLTPLKA	
8	KLTPLKKKLTALKA	Identical to clones 11 and 12
13	KLPLLKSKLLSLKA	

* Identified amino acid residues are shown in red.

Supplementary Table S3. Amino acid sequences of EGFR mutants and HLH peptides*

Clone name	Amino acid sequences	Ref.
	10 20 30 40 50	
Human EGF	NSDSECPLSHDGYCLHDGVCMYIEALDKYACNCVVGYIGERCQYRDLKWWELR	37–39
G12Q	----------Q----------	39
Y13W	----------W----------	39
H16D	----------D----------	39
Clone 114	SRG-K--P-------QG----------R---------A---------T--GR-	40
m28	----------G------K-V-R----------T--GP-	41
m123	--Y----P-Y----------R------S---------A---------R--GR-	41
	10 20 30 40	
HLH	QAWAELAALEMELAALEGGGGGGGKL--LK-KL--LKAGGGS	
2	DP I ES	
3	SS A SH	
5	NR H SF	
7	IC H TP	
8	TP K TA	
13	PL S LS	

*Replaced amino acid residues in enhanced EGF mutants (G12Q, Y13W, H16D, clone 114, m28, m123) are shown. Essential amino acids for EGFR binding are indicated in red. Boxes and underline in HLH sequence indicate α-helix region and loop region, respectively.

Specific delivery of microRNA93 into HBV-replicating hepatocytes downregulates protein expression of liver cancer susceptible gene MICA

Motoko Ohno[1,*], Motoyuki Otsuka[1,2,*], Takahiro Kishikawa[1], Chikako Shibata[1], Takeshi Yoshikawa[1], Akemi Takata[1], Ryosuke Muroyama[3], Norie Kowatari[3], Masaya Sato[1], Naoya Kato[3], Shun'ichi Kuroda[4] and Kazuhiko Koike[1]

[1] Department of Gastroenterology, Graduate School of Medicine, The University of Tokyo, Tokyo, Japan

[2] Japan Science and Technology Agency, PRESTO, Kawaguchi, Saitama, Japan

[3] Unit of Disease Control Genome Medicine, Institute of Medical Science, The University of Tokyo, Tokyo, Japan

[4] Graduate School of Bioagricultural Sciences, Nagoya University, Nagoya, Japan

[*] These authors contributed equally to this work

Correspondence to: *Motoyuki Otsuka* , ***email:*** *otsukamo-tky@umin.ac.jp*

Keywords: Hepatitis; Bionanocapsules; Drug delivery; Primary hepatocyte

Received: *June 13, 2014* ***Accepted:*** *June 24, 2014* ***Published:*** *June 26, 2014*

ABSTRACT

Chronic hepatitis B virus (HBV) infection is a major cause of hepatocellular carcinoma (HCC). To date, the lack of efficient in vitro systems supporting HBV infection and replication has been a major limitation of HBV research. Although primary human hepatocytes support the complete HBV life cycle, their limited availability and difficulties with gene transduction remain problematic. Here, we used human primary hepatocytes isolated from humanized chimeric uPA/SCID mice as efficient sources. These hepatocytes supported HBV replication in vitro. Based on analyses of mRNA and microRNA (miRNA) expression levels in HBV-infected hepatocytes, miRNA93 was significantly downregulated during HBV infection. MiRNA93 is critical for regulating the expression levels of MICA protein, which is a determinant for HBV-induced HCC susceptibility. Exogenous addition of miRNA93 in HBV-infected hepatocytes using bionanocapsules consisted of HBV envelope L proteins restored MICA protein expression levels in the supernatant. These results suggest that the rescued suppression of soluble MICA protein levels by miRNA93 targeted to HBV-infected hepatocytes using bionanocapsules may be useful for the prevention of HBV-induced HCC by altering deregulated miRNA93 expression.

INTRODUCTION

Hepatitis B virus (HBV) infection is a major global health problem, and more than 350 million people globally are chronic carriers of the virus [1]. A significant number of these carriers suffer from either liver failure or hepatocellular carcinoma (HCC) during the late stages of the disease [2]. In fact, chronic infection with HBV is responsible for 60% of HCC cases in Asia and Africa and at least 20% those in Europe, Japan, and the United States [3].

While nucleoside and nucleotide analogs have been applied in the attempts to suppress HBV replication [4, 5], complete elimination of HBV (including cccDNA) remains difficult [6, 7], and an increased understanding of HBV replication and pathogenesis at the molecular level is essential for clinical management of chronic HBV infection. However, the lack of appropriate cell culture systems supporting stable and efficient HBV infection has been a major limitation. Although transient transfection or viral transfer of HBV genes or genomes are used in the study of specific steps of the HBV cell cycle [8-12], they do not accurately reflect the biology of HBV infection and replication. Thus, humanized mice are used for hepatitis virus research [13-18]. Although these mice are useful, immune deficient, chimeric mice are difficult to handle

and maintain. Therefore, a more convenient *in vitro* system is required for HBV research.

Primary human hepatocytes can support the complete HBV life cycle *in vitro* [7, 19], but a major drawback is their limited availability. To overcome difficulties regarding availability, we used chimeric mice as sources of primary human hepatocytes, which grow robustly during the establishment of chimeric mice, due to continual liver damage induced by urokinase-type plasminogen activator (uPA) [14, 15].

Another shortcoming of utilizing primary human hepatocytes is their difficulty with gene transduction due to the low transfection efficiency of their primary cell-like nature. Efficient gene delivery methods will significantly improve studies on primary hepatocytes for HBV replication. In addition, cell-specific targeting is required for efficient drug delivery *in vivo*. As a specific gene delivery method to liver-derived cells, bionanocapsules (BNCs) consisted of HBV envelope L particles have been tested for the selective delivery of genes, drugs, or siRNAs into liver-derived cells [20, 21]. Because these BNCs are consisted of HBV L protein, they may be applicable for drug delivery to HBV-infected primary human hepatocytes.

MicroRNAs (miRNAs) are endogenous ~22-nucleotide RNAs that mediate important gene-regulatory events by base-pairing with mRNAs and activating their repression [22]. We previously reported that modifying the expression of miRNAs in liver cells can efficiently regulate the expression levels of the MHC class I polypeptide-related sequence A (MICA) protein [23], which we previously identified as a crucial factor for the susceptibility of hepatitis virus-induced HCC and possibly hepatitis virus clearance [24, 25]. While emerging evidence suggests that miRNAs play crucial roles in chronic HBV infection [26], the comprehensive changes in miRNA expression levels induced by HBV infection in human hepatocytes or in alternative systems reflecting HBV-infected hepatocytes have not been explored.

In this study, we infected primary human hepatocytes isolated from chimeric mice with HBV and identified the transcripts and miRNAs whose expression levels changed. We explored whether BNCs carrying synthesized miRNAs could successfully deliver miRNAs into primary hepatocytes and rescue the modulated miRNA expression due to HBV replication. We found that BNCs carrying synthesized miRNA93 could efficiently restore deregulated soluble MICA protein levels in the supernatant of HBV-replicating primary hepatocytes. These results suggest that miRNA93 delivery into HBV-replicating hepatocytes using BNC methods may enhance HBV immune clearance or suppress HCC by altering miRNA93 levels in HBV-infected cells.

RESULTS

Changes in expression levels of transcripts and miRNAs during HBV replication in human primary hepatocytes

We examined changes in transcript and miRNA expression levels during HBV infection and replication in hepatocytes. Primary human hepatocytes were used for maintainng HBV replication *in vitro*. We first isolated primary hepatocytes from humanized chimeric mice. To examine the infectivity of HBV into the primary hepatocytes *in vitro*, HBsAg and HBV-DNA levels in the cell culture supernatant were measured after the cells were infected with approximately 1.5×10^7 copies of HBV/well in a 24-well plate at day 0. Although both HBsAg and HBV-DNA levels transiently decreased at approximately day 3, levels of both started to increase and were maintained until after day 23 post-infection (Figure 1a and b). These results suggested that human primary hepatocytes isolated from chimeric mice can efficiently support HBV replication *in vitro*, which can be used as an efficient *in vitro* HBV replication system.

To examine comprehensive changes in mRNA and miRNA expression levels in HBV-infected hepatocytes, cells at day 7 post-infection were collected and subjected to cDNA as well as miRNA microarrays. Among 24,460 genes examined, 65 were significantly upregulated by more than 4-fold, and 29 were downregulated to less than 25% (Supplementary Table 1 and 2); however, more than 800 total genes were upregulated or downregulated if the thresholds of the changes were set at 2-fold and 1.5-fold, respectively (Figure 1c; complete datasets have been deposited as GEO accession number: GSE55928). Among the upregulated genes, those associated with the cytochrome family, such as CYP2A7, CYP2C8, CYP2A6, CYP3A4, changed significantly, which was consistent with previous reports [27, 28]. However, few inflammatory cytokines or genes associated with cell growth changed significantly. Based on these results, host factors related to innate immunity may not sense HBV (at least under these replicating conditions), suggesting that this system may mimic the status of hepatitis B patients before seroconversion, in whom inflammation seldom occurs regardless of the high viral load.

Regarding changes in miRNA expression levels during HBV replication, among 2,019 mature miRNAs, 35 were upregulated and 14 downregulated by an increase or decrease of more than two-fold (Figure 1d and Supplementary Tables 3 and 4; complete datasets have been deposited as GEO accession number: GSE55929). Among these miRNAs, miR93-5p was significantly downregulated during HBV replication by more than 50%. Since miRNA93 regulates the expression levels